



HAL
open science

Selective identification of cyclopentaring-fused PAHs and side-substituted PAHs in a low pressure premixed sooting flame by photoelectron photoion coincidence spectroscopy.

Xavier Mercier, Alessandro Faccinnetto, Sébastien Batut, Guillaume Vanhove, Dušan K Božanić, Helgi Rafn R Hrodmarsson, Gustavo A Garcia, Laurent Nahon

► To cite this version:

Xavier Mercier, Alessandro Faccinnetto, Sébastien Batut, Guillaume Vanhove, Dušan K Božanić, et al.. Selective identification of cyclopentaring-fused PAHs and side-substituted PAHs in a low pressure premixed sooting flame by photoelectron photoion coincidence spectroscopy.. *Physical Chemistry Chemical Physics*, 2020, 22 (28), pp.15926-15944. 10.1039/d0cp02740e . hal-03018681

HAL Id: hal-03018681

<https://hal.science/hal-03018681>

Submitted on 23 Nov 2020

HAL is a multi-disciplinary open access archive for the deposit and dissemination of scientific research documents, whether they are published or not. The documents may come from teaching and research institutions in France or abroad, or from public or private research centers.

L'archive ouverte pluridisciplinaire **HAL**, est destinée au dépôt et à la diffusion de documents scientifiques de niveau recherche, publiés ou non, émanant des établissements d'enseignement et de recherche français ou étrangers, des laboratoires publics ou privés.

1 **Title: Selective identification of cyclopentaring-fused PAHs and side-**
2 **substituted PAHs in a low pressure premixed sooting flame by photoelectron**
3 **photoion coincidence spectroscopy**

4
5 **Authors:** X. Mercier^{1*}, A. Faccinetto¹, S. Batut¹, G. Vanhove¹, D. K. Bozanic^{2†}, H. R.
6 Hrodmarsson^{2,‡}, G. A. Garcia², L. Nahon²

7
8 **Affiliations:**

9 ¹Université Lille, CNRS, UMR 8522 - PC2A - Physicochimie des Processus de Combustion et de l'Atmosphère, F-
10 59000 Lille, France,

11 ² Synchrotron SOLEIL, L 'Orme des Merisiers, St. Aubin, BP 48, 91192 Gif sur Yvette, France

12
13 *Correspondence to: Xavier Mercier (xavier.mercier@univ-lille.fr). Tel: + 33 3 20 43 48 04

14 [†]Current institutional address: Vinča Institute of Nuclear Sciences, University of Belgrade, P.O. Box 522, 11001
15 Belgrade, Serbia

16 [‡]Current institutional address: Laboratory for Astrophysics, Leiden Observatory, Leiden University, PO Box 9513,
17 NL-2300 RA Leiden, The Netherlands

18
19 **Abstract:**

20 This work reports on the selective on-line identification of polycyclic aromatic hydrocarbons
21 (PAHs) formed in a low-pressure methane sooting flame, carried out using the double imaging
22 Photoelectron Photoion Coincidence Spectroscopy method (i²PEPICO) on the DESIRS VUV
23 beamline at the synchrotron SOLEIL. Generally, this work demonstrates the capabilities of the
24 i²PEPICO method to identify PAHs in sooting flames, and in particular to distinguish
25 cyclopentaring-fused PAHs (CP-PAHs) and side-substituted PAHs from their benzenoid isomers.
26 Experimental threshold photoelectron spectra of four CP-PAHs: acenaphthylene (C₁₂H₈, 152 *m/z*),
27 acenaphthene (C₁₂H₁₀, 154 *m/z*), fluoranthene (C₁₆H₁₀, 202 *m/z*) and benzo(ghi)fluoranthene
28 (C₁₈H₁₀, 226 *m/z*) are also reported for the first time.

29

30 **Keywords:** threshold photoelectron spectroscopy (TPES), electron/ion coincidence, polycyclic

31 aromatic hydrocarbons (PAHs), soot, nucleation

32 **1. Introduction**

33 Soot particles released at the exhaust of combustion processes are subject to special attention
34 because of their well-documented detrimental impact on the human health and environment. Soot
35 particles in the atmosphere are at the origin of allergic rhinitis and other affections of the
36 respiratory system¹. Many hydrocarbons adsorbed at the surface of soot particles and formed
37 during the combustion process are known to be toxic and to have mutagenic and/or carcinogenic
38 health effects^{2,3}, and the inhalation of soot particles has been correlated to a wide variety of acute
39 and chronic diseases⁴. In the environment, especially when released in the high troposphere by
40 aeronautic jet engines for instance, soot particles impact the radiative forcing of the atmosphere as
41 they can absorb and scatter the solar radiation (direct effect) or act as cloud/ice condensation nuclei
42 and trigger the formation of persistent clouds (indirect effect), thereby affecting the local
43 climate^{5,6}. The detailed chemical characterization of soot particles can therefore provide crucial
44 information to better assess their toxicity and atmospheric reactivity, and furthermore, help to
45 clarify their formation process, which so far is not completely understood.

46 The formation of soot particles in flames is known to be strongly correlated to reaction
47 pathways involving polycyclic aromatic hydrocarbons (PAHs), which are considered the main
48 precursors of soot particles. Although the growth of PAHs is widely accepted to be driven by the
49 HACA mechanism⁷ (Hydrogen Abstraction Acetylene Addition), alternative reaction pathways
50 have also been suggested⁸⁻¹³. In order to evaluate the relative importance of these pathways,
51 experimental data are needed to, firstly, unambiguously identify the chemical species involved in
52 the soot formation process, and secondly, to measure their in-flame concentrations. However,
53 recent atomic force microscopy experiments¹⁴ demonstrated that the growth process of PAHs
54 naturally results in the formation of a variety of structural isomers that can be found adsorbed on
55 the soot particles surface. At a given mass, structural isomers of PAHs can be very difficult to
56 discriminate with traditional analytical techniques as their number rapidly increases with the

57 number of carbon atoms in the molecule¹⁵. In-situ laser based methods such as laser induced
58 fluorescence (LIF) can generally provide qualitative data about PAH formation in flames, as well
59 as the PAH class size and their localization in the flame¹⁶⁻²², but such methods are incapable of
60 unfolding the contributions of individual species. It has been recently shown that better
61 discrimination can be achieved by using relatively simple spectral models for the interpretation of
62 the experimental fluorescence spectra that rely on the use of tabulated fluorescence spectra of
63 individual PAHs^{23,24}. Not only these methods allow the identification of the main PAHs formed in
64 flames, but in particularly favorable cases they can even distinguish between structural isomers
65 such as pyrene and fluoranthene. However, such approaches do not yet allow quantitative
66 measurements. The determination of mole fraction profiles of PAHs in flames by LIF indeed
67 requires ex-situ measurements, such as those provided by complex laboratory setups like Jet-
68 Cooled Laser Induced Fluorescence (JCLIF)^{25,26}. However, JCLIF requires fine adjustment of the
69 excitation laser wavelength to a resonant transition of a specific target PAH, which limits the
70 measurement capability to a few PAHs having well-known spectral properties, and to only one
71 isomeric structure at a time.

72 In comparison, mass spectrometry-based methods based on time-of-flight are multiplex in
73 mass, and allow the simultaneous measurement of all the molecular species in the sample but can
74 generally not distinguish structural isomers. In addition, the high ionization energies used in
75 typical setups based on electron impact lead to complex fragmentation patterns that complicate the
76 identification of the parent ions. In this context, tunable vacuum ultraviolet (VUV) radiation, such
77 as the one provided by synchrotron-based techniques, is an attractive way to obtain selective PAHs
78 concentration profiles in flames because of its ability to distinguish structural isomers²⁷⁻³⁰ via
79 spectral discrimination, and to avoid or limit the amount of fragmentation by ionizing close to the
80 threshold. Different research groups highlighted the capabilities of such techniques for the
81 selective and quantitative measurement of species formed in rich flames³¹⁻³⁴. In the cited works,

82 unknown species are identified through their photoionization efficiency (PIE) curve, which
83 consists of the integrated ion signal against the photon energy. The first ionization of PAHs
84 commonly leads to the formation of stable molecular cations that can be detected independently
85 by mass spectrometry. Therefore, a PIE curve recorded for a specific mass with tunable
86 Synchrotron Radiation (SR) in the range of, and immediately above the first ionization energy of
87 PAHs ($IE = 7-11.5$ eV) in principle allows the identification of structural isomers once their
88 individual spectral contribution are known^{28,31,34-36}. However, these curves integrate over all
89 available states of the cation at a given photon energy, and therefore lack sufficient spectral
90 structures to deliver an unambiguous interpretation, especially when several isomers coexist at the
91 same m/z and have close IE values. This is notably the case of $m/z = 152$, studied in this work,
92 which is generally associated to four different main isomers³⁷ in flame investigations: biphenylene
93 ($IE=7.58$ eV, ) , acenaphthylene ($IE=8.02$ eV, ) , 1-ethynylnaphthalene ($IE=8.11$ eV, )
94 and 2-ethynylnaphthalene ($IE=8.03$ eV, ). In this case, the distinction between
95 acenaphthylene and 2-ethynylnaphthalene based only on their PIE curves is impossible. We note,
96 however, that in some cases identification can be greatly helped by the appearance of
97 autoionization features in the PIE curves, such as the ones seen for coronene³⁸.

98 As a first approximation, ignoring autoionization resonances, a PIE curve corresponds to the
99 integral of the photoelectron spectrum (PES) at a given photon energy and therefore contains much
100 less sharp spectroscopic features, i.e. possesses a much weaker analytical ability in disentangling
101 structural isomer ions detected at the same m/z . For this reason, photoelectron-photoion
102 coincidence spectroscopy (PEPICO) has been demonstrated in the last years to be a powerful tool
103 for the identification of structural isomers in complex gas-phase environments such as flames,
104 combustion reactors and oxidation chambers³⁹⁻⁴⁷. This technique enables the recording of
105 photoelectron spectra (PES) of the mass-selected ionized detected species. Because of the richer
106 vibronic structure as compared to PIE curves, the PES acts as a unique fingerprint providing

107 unambiguous information about its structure^{43,48}. Such a fine analysis of complex mixtures via
108 mass-selected PES is based upon the comparison with either known experimental PES of pure
109 compounds or, alternatively, PES obtained from ab-initio calculations. Notably, Felsmann et al.⁴¹
110 demonstrated the capabilities, including the sensitivity, of the double imaging photoelectron
111 photoion coincidence spectrometer *i*²PEPICO technique for the identification of different
112 structural isomers formed in dimethyl ether and cyclopentene flames. They identified for the first
113 time without ambiguity in the low pressure cyclopentene flame, the contributions of 1-penten-3-
114 yne in competition with the much larger signal of 1,3-cyclopentadiene. Different other aromatic
115 species up to 128 *m/z* were also detected.

116 The aim of this work is to explore the capabilities of the *i*²PEPICO method for the detection of
117 PAHs in sooting flames, more specifically focusing on the identification of gas phase PAHs
118 isomers formed in the nucleation region of a sooting flame. This study has been carried out on the
119 DESIRS VUV beamline at the SOLEIL synchrotron by using the permanent *i*²PEPICO-based
120 experimental setup SAPHIRS, which was coupled to a low pressure premixed CH₄/O₂/N₂ sooting
121 flame stabilized at the pressure $p=26.66$ kPa (200 torr), with an equivalence ratio $\phi=2.32$. This
122 flame was chosen for several reasons. First, it has already been the subject of several studies by
123 some of the co-authors dedicated to PAHs and soot formation^{25,49–54} with a variety of diagnostics,
124 therefore providing an ideal benchmark case for the present work. Second, this flame is a lightly
125 sooting flame characterized by a soot volume fraction profile reaching values of the order of a few
126 ppb in the burnt gases⁵³. The study of sooting flames with the *i*²PEPICO setup introduces an
127 additional difficulty for sampling measurements in comparison to the non-sooting flames studies
128 reported above. Because of the formation of soot particles, the clogging of the sampling probe
129 becomes a critical issue during the recording of photoelectron spectra that can take up to several
130 hours. The choice of this lightly sooting flame was also aimed at limiting this issue. Note, however,
131 that contrary to PIE curves where the photon energy needs to be scanned and thus a high reactor

132 stability is required, fixed-photon energy photoelectron spectroscopy can also be recorded with
133 the i^2 PEPICO setup. This approach can be much faster and overcomes the need for stability, albeit
134 at the expense of energy resolution, as discussed further in the text and demonstrated in the context
135 of flames^{41,43}.

136 To demonstrate the capability of the i^2 PEPICO setup for PAH measurements and isomer
137 discrimination in sooting flames, we specifically focused on the nucleation region of the flame,
138 i.e. the zone where the first nascent soot particles (NSPs) are formed. One specific outcome of this
139 work was to clearly highlight the formation of cyclopentaring-fused-PAHs (CP-PAHs) whose
140 structure contains five-membered carbon rings, which have already been proposed in the literature
141 to be important intermediates on the formation of NSPs^{11,12,55–58}. CP-PAHs often share the same
142 molecular formula as six-membered ring PAHs, and are thus impossible to distinguish with
143 common mass spectrometry setups. Moreover, we were also interested in revealing the presence,
144 or absence, of side-substituted PAHs in the sampled gases. The i^2 PEPICO setup provides a unique
145 possibility to record the PES for each of the peaks on the mass spectra simultaneously, allowing
146 the identification of the formed PAHs via their electronic fingerprints, provided that individual
147 PES of the detected species are known. PES of small hydrocarbons are globally well documented
148 in the literature, which makes their identification straightforward. However, the number of isomers
149 quickly increases with the size of the molecule making the identification of larger molecules, such
150 as PAHs more complex. In particular, the selective identification of some of these PAH isomers
151 required the measurement of the PES of several pure CP-PAHs which not available in the literature
152 at the time of our experiments. Hence, the PES of fluoranthene ($C_{16}H_{10}$, 202 m/z), acenaphthylene
153 ($C_{12}H_8$, 152 m/z), acenaphthene ($C_{12}H_{10}$, 154 m/z) and benzo(ghi)fluoranthene ($C_{18}H_{10}$, 226 m/z)
154 are also reported for the first time in this paper.

155 The experimental setup we used can be operated in two modes: (1) the threshold-PES mode
156 enabling the determination of the PES by scanning the photon energy while selecting only quasi-

157 zero kinetic energy electron and (2) the PES mode in which the full PES is encoded into a single
158 electron image recorded at fixed photon energy. In both modes all the masses are acquired
159 simultaneously, providing mass-selected TPES and PES data. A comparison between the results
160 obtained with these two different modes of operation is also reported in this paper. Benefits,
161 capabilities and limitations of both modes for PAHs, side-substituted PAHs and CP-PAHs
162 identification are then discussed.

163

164 2. Experimental Setup

165 2.1 Experimental setup used for the determination of PES and PIE curves of 166 acenaphthene, acenaphthylene, fluoranthene and benzo(ghi)fluoranthene

167

168 In order to enable the analysis of specific detected masses and especially highlight the presence
169 of some CP-PAHs, the measurement of PES and PIE curves of four CP-PAHs currently missing
170 in the literature and likely formed in sooting flames has been carried out in this work. These species
171 of interest were acenaphthylene ($C_{12}H_8$, 152 m/z), acenaphthene ($C_{12}H_{10}$, 154 m/z), fluoranthene
172 ($C_{12}H_{10}$, 202 m/z) and benzo(ghi)fluoranthene ($C_{18}H_{10}$, 226 m/z).

173 The spectra of these species have been recorded by depositing the pure CP-PAHs (98-99%
174 purity, Aldrich) in an in-vacuum stainless-steel oven. The experimental device has been already
175 described in detail in a previous work⁵⁹. He (0.5 bar) was flowed across the oven to carry the PAH
176 vapor before expansion through a 70 μm nozzle to form a molecular beam which crossed the two
177 consecutive skimmers of the multipurpose SAPHIRS chamber⁶⁰ before reaching the ionization
178 region. The temperature of the oven has been adjusted according to each CP-PAHs to generate a
179 vapor pressure enabling the recording of PES with Signal-To-Noise ratio $\text{SNR} > 3$. *Table 1* shows
180 the working temperatures and consumption of the four compounds studied in this work. The

181 temperatures of the nozzle and oven were optimized to get around 6000 events/second at the
 182 highest scan energy, which resulted in high quality scans with minimal consumption.
 183

m/z	Molecular formula	Compound	Structure	Temperature of oven / nozzle (°C)	Total consumption (mg)
152	C ₁₂ H ₈	Acenaphthylene		53/63	60
154	C ₁₂ H ₁₀	Acenaphthene		55/65	50
202	C ₁₆ H ₁₀	Fluoranthene		120/130	1215
226	C ₁₈ H ₁₀	Benzo(ghi)fluoranthene		120/135	12

184
 185 *Table 1: Experimental conditions for PES and PIE curves measurements*

186
 187 The undulator-based DESIRS beamline⁶¹ was set to provide $\sim 5 \times 10^{12}$ photons/sec with a
 188 spectral bandwidth of 10 meV at 10 eV. A pressure of 0.14 mbar of Kr filled the gas filter to ensure
 189 spectral purity in our energy range⁶² by suppressing the high harmonics of the undulator. The
 190 energy scales were absolutely calibrated using either the 4p⁵ 5s(3/2) Kr absorption line⁶³ from the
 191 gas filter, as visible in the total ion yields, or the third-order ionization energy of He as reported in
 192 the NIST database. The energy scan data have been normalized by the photon flux measured with
 193 an AXUV100 photodiode from International Radiation Detectors, Inc.

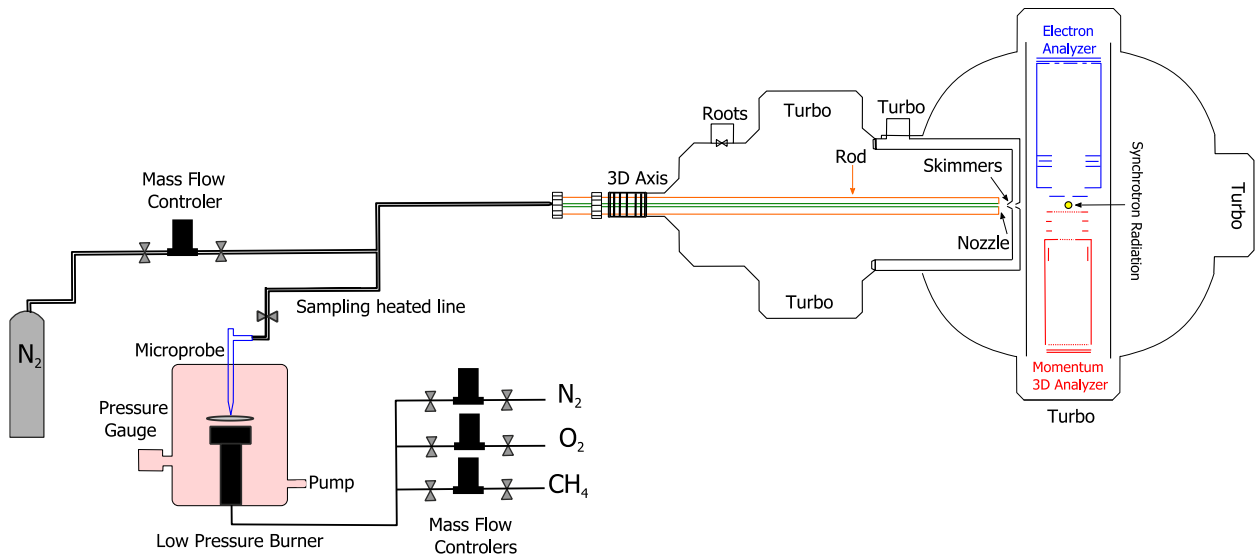
194 The DELICIOUS3 i²PEPICO spectrometer⁶⁴, which couples a VMI spectrometer on the
 195 electron side and a 3D-momentum imager spectrometer on the ion side, was used in the
 196 coincidence mode to obtain the photoelectron images correlated to a given ion mass and position
 197 at each scan point (or fixed photon energy), with a continuous extraction field of 88 V/cm. Note
 198 that the selection of a given ion arrival position in the detector (ion Region Of Interest, or ion ROI)
 199 ensures that only molecules originated in the flame or from HAP vaporization, and thus having a
 200 net velocity along the molecular beam, are considered, decreasing the background signal coming

201 from the 10^{-7} mbar base pressure of the ionization chamber⁶⁵. TPES were obtained with the Slow
 202 Photoelectron Spectroscopy method described previously⁶⁶. For the standards mentioned in **Table**
 203 **I**, photoelectrons from 0 to 70 meV were used to build the TPES, which provided an electron
 204 kinetic energy resolution of 10 meV as measured on the third-order ionization of He, leading to an
 205 overall resolution of 14 meV and an overall absolute accuracy for the *IE* determination of
 206 0.003 eV.

207

208 **2.2 Flame sampling experiment**

209 A schematic representation of the experimental setup used for this work is reported in **fig. 1**.



210

211

Figure 1: Experimental Setup

212

213 As mentioned in the introduction, we investigated a low pressure premixed sooting flame of
 214 methane/oxygen/nitrogen characterized by a fuel-to-oxidizer equivalence ratio $\phi = 2.32$. The
 215 pressure inside the vessel was controlled and kept constant at 26.66 kPa (200 torr) thanks to an
 216 automatic pressure regulation valve. More details about this flame and the low pressure vessel
 217 arrangement can be found in previous publications^{25,26}. The experimental flame conditions are
 218 reported in **Table 2**.

ϕ	C/O	x_{CH_4}	x_{O_2}	x_{N_2}
2.32	0.58	0.462	0.398	0.14

Table 2: Composition of the studied flame. The total flow rate was 3.96 L/min STP.

219
220
221
222 During the flame experiments, species were continuously extracted from the flame through a
223 thin microprobe having a 300 μm aperture diameter. The pressure inside the line was kept constant
224 to 10 ± 0.01 mbar. The whole transfer line from the microprobe down to the skimmer located in
225 the SAPHIRS chamber was heated up to 140 $^{\circ}\text{C}$ to limit the condensation of the PAHs as discussed
226 in a previous work⁶⁷. Extracted species were directly expanded in the SAPHIRS chamber through
227 a nozzle with an orifice aperture of 500 μm . This relatively large orifice was used to optimize the
228 SNR and the sensitivity of the measurement at the cost of a less efficiently cooled and collimated
229 supersonic beam. The supersonic beam was then double skimmed before finally crossing the
230 synchrotron beam at a right angle in the ion source of the i^2 PEPICO spectrometer. The position of
231 the nozzle with respect to the ionization beam was aligned and optimized by using a dedicated N_2
232 line.

233 With this setup, we implicitly made the choice to limit the detection to stable species only.
234 Indeed, the use of a microprobe, instead of a sampling cone and skimmer device as usually
235 implemented for generating a molecular beam, does not allow the capture of radicals. In return,
236 this system offers a much lower detection limit than typical molecular beam mass spectrometry
237 setups. We estimated our detection limit in the order of 0.1 ppm, i.e. at least one order of magnitude
238 lower than the typical sensitivity of 1-10 ppm of molecular beam mass spectrometry setups
239 reported in the literature^{31,32,68,69}. This value was estimated from the comparison with quantitative
240 measurements carried out by JCLIF in the same flame²⁵ reporting peak mole fractions of pyrene
241 and fluoranthene around 0.4 and 0.1 ppm.

242 In this work, we carried out either the recording of ion mass- and ROI-selected PES data at
243 fixed photon energy (denoted as PES spectra in figures) and/or TPES spectra by scanning the
244 photon energy⁶⁶. PES typically required around 30 minutes of data acquisition to get a satisfactory
245 SNR (typically SNR>3). The TPES mode greatly improves the spectral resolution but requires an
246 acquisition of a few hours because the photon energy needs to be scanned. For the flame
247 experiments, the photoelectron window used to obtain the TPES was increased to 200 meV to
248 achieve a better SNR, leading to an overall energy resolution of 35 meV.

249 Most PES experiments were performed at 8 eV to favor the ionization of small PAHs and limit
250 fragmentation of the parent cations. However, we also report a few spectra recorded at higher *IE*
251 up to 9-10 eV, in order to broaden the range of detected species towards small aromatic and
252 aliphatic compounds.

253 As mentioned above, we focused our measurements on the beginning of the soot nucleation
254 zone of the flame as determined in previous work^{25,54}, which corresponds to a region located from
255 height above the burner (HAB) 9 to 15 mm where the temperature of the flame has been
256 determined be nearly constant around 1760 ± 20 K⁵². Note that around 80 different peaks in the 40-
257 252 *m/z* range have been detected in this zone.

258

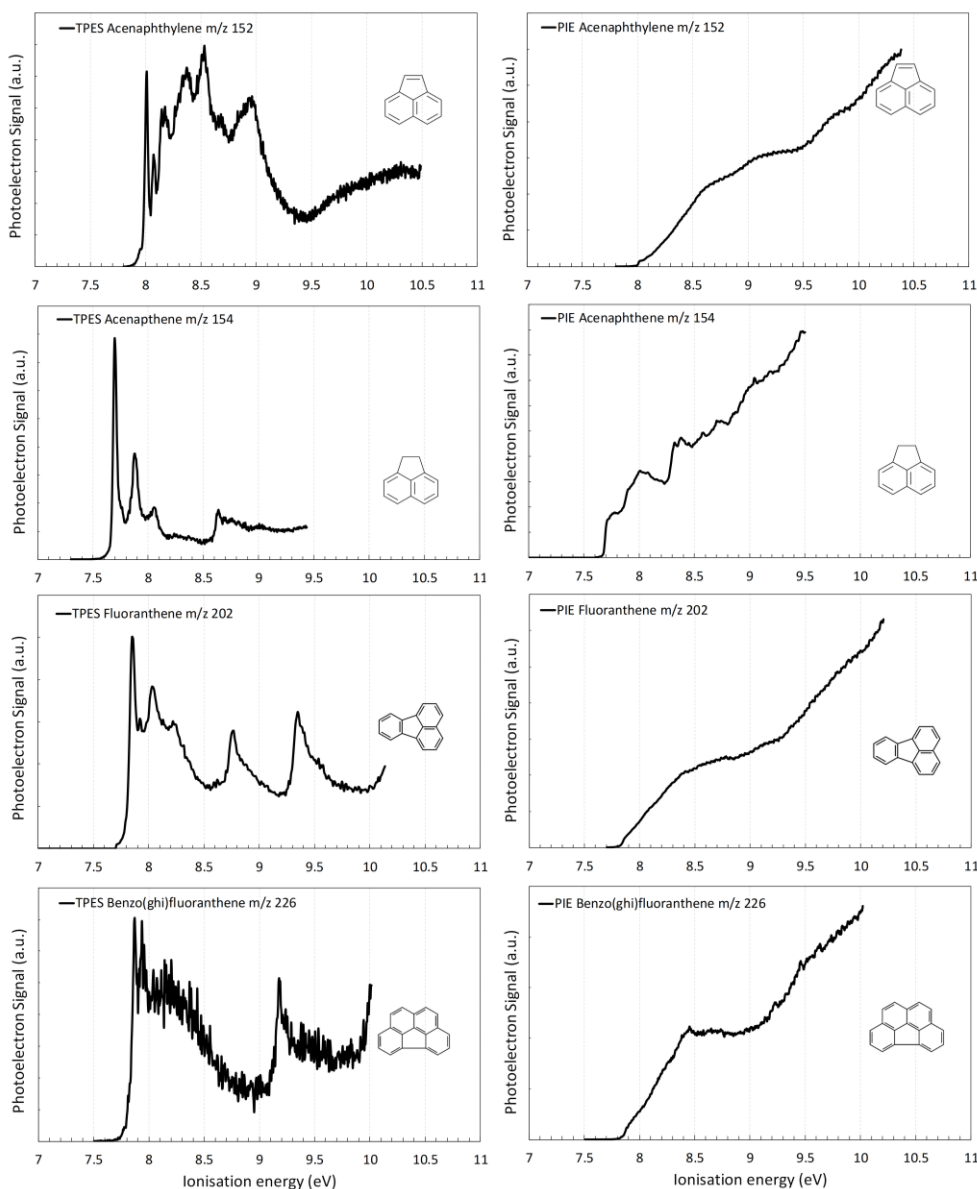
259 3. Results and discussion

260

261 3.1 Measurements of the reference PES and PIE curves of acenaphthene, 262 acenaphthylene, fluoranthene and benzo(ghi)fluoranthene

263 The TPES and PIE curves recorded for the four CP-PAHs are shown in *fig.2*. Note that all the
264 data shown correspond to the parent ion selection. No fragmentation channels have been identified
265 in the TOF mass spectra for any of the four PAHs considered here, up to 10.5 eV. While *IE* values
266 have already been published in the literature for acenaphthene, acenaphthylene and fluoranthene³⁷,

267 the hereby reported TPES for these species correspond to new and unique reference spectra to the
268 best of our knowledge. Concerning benzo(ghi)fluoranthene, neither *IE* values nor PES or PIE
269 curves were available in the literature. Note that the SNR is inferior in this last spectrum than in
270 the other ones due to the much lower vapor pressure of benzo(ghi)fluoranthene. However, the
271 recorded spectrum still highlights clearly distinguishable and characteristic vibronic structures.
272 Such spectra are likely to be used for the identification of these species in various applications
273 including combustion but also other scientific fields like astrophysics. The unique character of
274 these new data remains therefore of significant interest beyond the scope of combustion studies.
275 Notably, the spectrum of fluoranthene, which is a structural isomer of pyrene, potentially remains
276 of great interest for both these communities considering the importance of pyrene in rich flame
277 chemistry and interstellar medium. Although pyrene itself has not yet been discovered in any
278 interstellar media, PAHs and PAH cations remain very astrophysically relevant. Kim et al.⁷⁰
279 reported that the infrared spectrum of the pyrene cation very closely resembles the interstellar
280 unidentified infrared emission bands. Furthermore, this work also opens a new way to individually
281 identify these PAHs in interstellar ice analogs and carbonaceous chondrites^{71,72}.
282



283

284

Figure 2: TPES (left column) and PIE curves (right column) of the four studied PAHs

285

286

287

288

289

290

291

292

The four measured TPES show strong distinguishable spectral features from which it is possible to extract the corresponding adiabatic ionization energy (IE_{ad}). IE_{ad} values are important as they are widely used to identify structural isomers in VUV-photoionization mass spectrometry experiments. In this work, the experimental IE_{ad} have been measured by fitting a Gaussian peak to the first transition of each spectrum, which is also the most intense band, meaning that there is little geometric change of the molecular structure upon ionization (favorable FC factors), which is typical of PAHs^{38,73,74}. The determined values, from the maximum of the Gaussian fitting function,

293 are reported in the first column of *table 3* and compared to measured values provided by the
 294 literature and referenced in the NIST Webbook. Note that for the three components for which IE_{ad}
 295 was previously known, our data provides an increased accuracy on the values.
 296

m/z	Molecular formula	Compound	IE_{ad} (eV)					
			This work			Literature		
152	C ₁₂ H ₈	Acenaphthylene	8.012±0.003	8.02±0.04 ^a	8.22±0.01 ^b			
154	C ₁₂ H ₁₀	Acenaphthene	7.700±0.003	7.68±0.05 ^c	7.73±0.01 ^b	7.66 ^d	7.76±0.03 ^e	7.82±0.04 ^a
202	C ₁₆ H ₁₀	Fluoranthene	7.860±0.003	7.90±0.1 ^f	7.95±0.04 ^a	7.80±0.01 ^b	7.72 ^g	
226	C ₁₈ H ₁₀	Benzo(ghi)fluoranthene	7.874±0.003					

297

298 *Table 3: Determined first adiabatic ionization energy compared to referenced values³⁷*

299 ^aBoschi et al.⁷⁵, ^bDewar et al.⁷⁶, ^cMautner et al.⁷⁷, ^dKinoshita et al.⁷⁸,

300 ^eHeilbronner et al.⁷⁹, ^fLing and Lifshitz⁸⁰, ^gSlifkin and Allison⁸¹

301

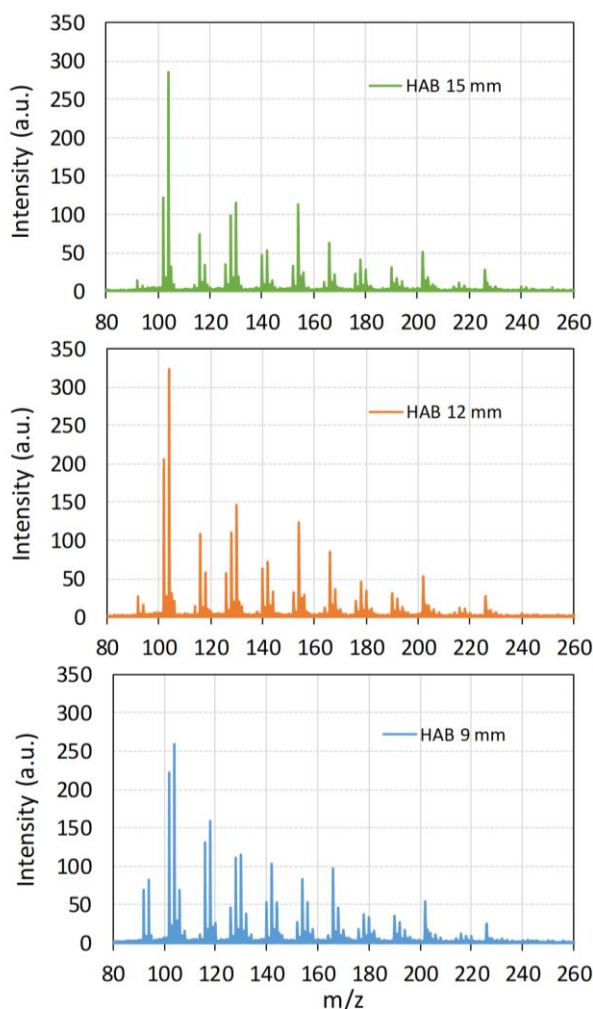
302 As can be seen in *table 3*, although for the most part our data agree with the literature values
 303 within the uncertainty, differences in IE_{ad} of more than 100 meV can be observed, which show
 304 potential deficiencies in the existing databases and the need of upgrading these values to meet the
 305 requirements of modern analytical experiments, especially in the context of species identification
 306 in complex mixtures.

307 Beyond the IE values, the overall shape of the TPES is relevant for the analysis of combustion
 308 processes, especially for the ground electronic state (typically over the first 1-1.5 eV above IE_{ad}).
 309 Without entering into a detailed analysis, which is beyond the scope of this work, the FC envelope
 310 of the ground electronic state of the four species shows quite a rich vibrational structure which is
 311 a molecular fingerprint for the analysis of complex mixtures. As discussed above, TPES

312 fingerprints are much sharper and molecule-specific than the PIE step functions (especially for
313 acenaphthylene and fluoranthene) and are therefore more appropriate as reference functions for
314 fitting the experimental data obtained from the analysis of complex mixtures.

315 316 **3.2 Implementation of the i²PEPICO setup for the identification of PAHs formed in** 317 **flames**

318 *Figure 3* shows a zoom of the mass spectra recorded at a fixed photon energy of 8 eV and for
319 three distinct sampling HABs (9, 12 and 15 mm above the burner) corresponding to the nucleation
320 zone of the flame. Around 80 different peaks, ranging from 40 to 252 m/z , have been detected.



321
322 *Figure 3: Zoom of the mass spectrum of the flame acquired at photon energy 8 eV*
323 *for different heights above the burner.*

324 Some peaks consistent to CP-PAHs and side-substituted PAHs can be noted in *fig. 3* at 152
325 m/z ($C_{12}H_8$), 154 m/z ($C_{12}H_{10}$), 166 m/z ($C_{13}H_{10}$), 190 m/z ($C_{15}H_{10}$), 202 m/z ($C_{16}H_{10}$), 216 m/z
326 ($C_{17}H_{12}$), 226 m/z ($C_{18}H_{10}$), and 252 m/z ($C_{20}H_{12}$). As mentioned above, the exhaustive analysis of
327 all detected masses is beyond the scope of this work, and here we focus on those for which this
328 study can offer the most interesting methodological and mechanistical information, as discussed
329 below.

330 To this end, the **remaining** of this section is organized in two main parts. The first one is
331 dedicated to the implementation of the i^2 PEPICO setup for the identification of small aromatic
332 species well known to be formed in sooting flames. The objective of this first part is to check the
333 performance of the i^2 PEPICO apparatus for this relatively new task in the context of sooting flames
334 studies. In the second part, we focus on the study of four different detected masses in our flame,
335 expected to correspond to moderate-sized PAHs that are very likely involved in the soot formation
336 mechanisms. These species correspond to 152 m/z ($C_{12}H_8$), 154 m/z ($C_{12}H_{10}$), 202 m/z ($C_{16}H_{10}$)
337 and 226 m/z ($C_{18}H_{10}$).

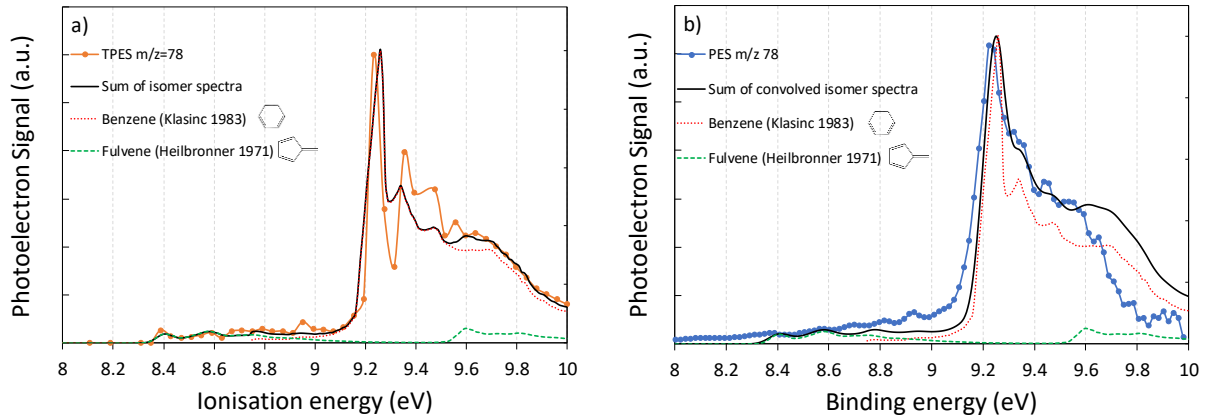
338 The identification method we used relies on the analysis of spectral structures of the
339 experimental TPES measured at different HAB in the nucleation region of the flame. The
340 identification of the species corresponding to the measured spectral structure is carried out by
341 comparing reference PES of individual PAHs (provided by the literature or from this work) with
342 the one acquired in the flame experiments. **To perform these comparisons, it has been necessary**
343 **to adjust the spectral resolution of the reference spectra when they were recorded with a better**
344 **spectral resolution than the experimental spectra. This has been carried out by convolving the**
345 **reference spectra provided by the literature to a Gaussian function to enlarge the spectral structures**
346 **of these spectra. The shape of the Gaussian function has been systematically adjusted according**
347 **to the resolution of the reference spectra, which came from different sources, in order to get the**
348 **best match with our experimental spectral structures.**

349 **3.2.1 Analysis of the species at 78 m/z (C_6H_6)**

350 Benzene is a species of great interest for soot formation as it plays a major role in the initiation
351 of the HACA mechanism. However, benzene is not the only isomer possibly detected in sooting
352 flames at 78 m/z . Fulvene, which has already been observed in rich flames⁸², is another likely
353 candidate that has been taken into account to analyze this spectrum. The measured TPES and PES
354 corresponding to 78 m/z are reported in **fig. 4a and 4b**. The simulated spectrum (black line),
355 calculated on the basis of the reference spectra of benzene⁸³ (grey dotted line) and fulvene⁸⁴ (grey
356 dashed line), is also reported on these figures. Due to the poorer spectral resolution of the PES in
357 comparison with the TPES, we intentionally degraded the simulated spectrum reported in **fig.4b**
358 using the procedure described by Felsmann et al.⁴¹ for previous comparable analyses. The PES has
359 been measured with the sampling probe in the sooting flame positioned at HAB = 12 mm, at a
360 fixed photon energy of 10 eV. This is the reason why the PES appears truncated, reaching a zero
361 value at 10 eV.

362 The acquisition time for this PES was approximately 30 minutes. The TPES reported in **fig.4a**
363 required the fine scanning of the ionization energy from 7.2 to 10 eV with a step of 0.04 eV. This
364 relatively large step has been chosen to limit the acquisition time to 6 hours. Both TPES and PES
365 clearly show an intense peak at 9.23 eV, in excellent agreement with the *IE* value of 9.24 eV of
366 the 0-0 vibrational transition of benzene reported in the literature⁸⁵, followed by a series of less
367 intense vibrational progressions. Also visible in these spectra, especially the TPES, is a series of
368 weak spectral features between 8.3 and 9.0 eV before the occurrence of the first benzene peak.
369 This structure is in good agreement with the vibrational structure of the electronic ground state of
370 fulvene characterized by two main peaks at 8.36 eV and 8.52 eV⁸⁵. The best adjustment we found
371 between the experimental spectrum (orange line) and the simulated one (black lines) in **fig.4** has
372 been obtained for relative contributions of benzene and fulvene of 90% and 10%, respectively.
373 This analysis therefore provides clear evidence of the formation of benzene in the nucleation zone

374 of the flame, in competition with fulvene with a much lower apparent signal ratio. This information
 375 is however less explicit in the PES reported in *fig.4b* due to the choice of the ionization energy
 376 which truncates the higher binding energy part of the spectrum.



377
 378 **Figure 4: TPES and PES (recorded at 10 eV) of 78 m/z at HAB=12 mm.**

379 **Comparison with a simulated spectrum (in black) corresponding to the sum of reference PES of benzene and**
 380 **fulvene for a signal ratio of 90:10.**

381
 382 It is to be noted that, in a previous study, the mole fraction of benzene was determined around
 383 85 ppm at this HAB in this flame by JCLIF²⁶. **Based on this experimental value, the concentration**
 384 **of fulvene can be determined from the relative intensities of the two spectra and the knowledge of**
 385 **the ionization cross section at 10 eV. Hence the mole fraction of fulvene X_f can be related to the**
 386 **benzene mole fraction X_b according to the formula:**

$$387 \quad X_f = X_b \frac{\sigma_{ib} S_f}{\sigma_{if} S_b} \quad \text{Eq.1}$$

388 where σ_{ib} and σ_{if} correspond to the benzene and fulvene ionization cross sections at 10 eV and
 389 S_f/S_b corresponds to the relative signal ratio of the contributions of fulvene and benzene. The
 390 absolute cross-section of benzene at 10 eV has been measured at 25 Mb^{86,87}, while for the fulvene
 391 only an estimated value of 35 Mb is found in the literature⁸⁸. These values lead to an estimated
 392 mole fraction of fulvene around 7 ppm at 12 mm HAB.

393 Note that the PES, which requires 12 times less time than the recording of the TPES scan, still
394 provides an adequate resolution and sensitivity for the detection of benzene in these conditions,
395 with the added advantages of not needing a stable sample, or tunable light, as discussed by Krüger
396 *et al.*⁴³ However, the degraded spectral resolution renders the identification of fulvene somewhat
397 less certain.

398

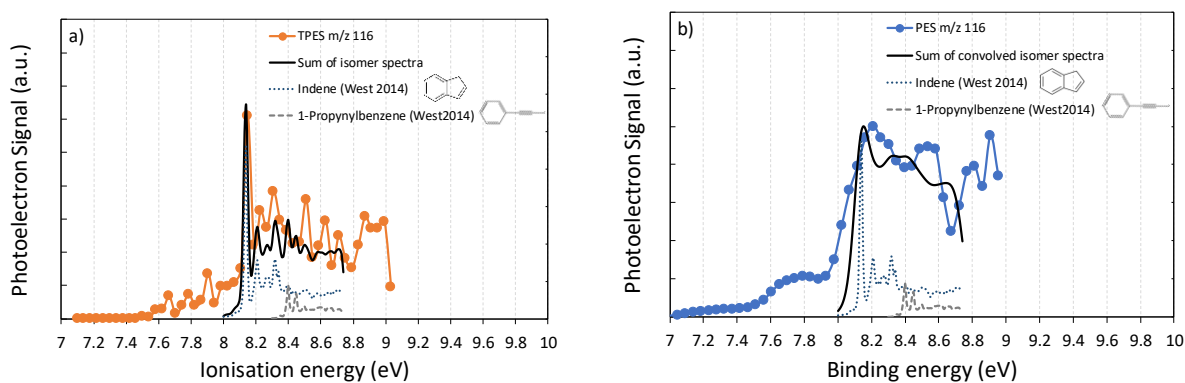
399 **3.2.2 Analysis of the species at 116 m/z (C_9H_8)**

400 This peak, commonly detected in sooting flames, potentially corresponds to indene, i.e. the
401 lightest CP-PAHs consisting of one six-member and one five-member ring. The identification of
402 this species by mass spectrometry methods is not trivial because of the several isomers coexisting
403 at this m/z , the most important of which being 1-propynylbenzene and the three ethynyl-methyl-
404 benzenes^{31,41}. *IE*s of 8.14 eV⁷⁶ and 8.41 eV⁸⁹ have been reported for indene and 1-propynylbenzene
405 respectively, while the *IE* values of 1-ethynyl-4-methylbenzene, 1-ethynyl-3-methylbenzene and
406 1-ethynyl-2-methylbenzene are 8.48, 8.63 and 8.61 eV⁸⁹. We show in **fig. 5a and 5b** the
407 comparison of experimental TPES and PES obtained at HAB = 15 mm with reference spectra for
408 pure indene and 1-propynylbenzene⁹⁰. As in the case of benzene detection, the TPES in **fig. 5a**
409 required a 6 hours long scan while the PES reported in **fig. 5b** has been recorded with a much
410 shorter acquisition time of approximately 30 minutes. The spectral resolution of both reference
411 spectra has been adjusted in order to match our experimental conditions. This has been done by
412 convolving the reference spectra with a Gaussian function according to the protocol previously
413 described in Felsmann *et al.*⁴¹

414 Although the TPES of indene reported in **fig. 5a** seems in itself able to explain our spectrum,
415 we also considered the potential contribution of the only other isomer for which the TPES has been
416 reported, 1-propynylbenzene. The indene and 1-propynylbenzene contributions associated to the
417 simulated spectra have been found to be 83% and 17%, respectively. However, it is possible that

418 minor contributions of other structural isomers are present on this spectrum. We notably observe
419 a slight increase in signal around 8.5 eV which might highlight the presence of 1-ethynyl-4-
420 methylbenzene, a species for which no reference spectrum is currently available. Moreover, no
421 correspondence could be found either for the small spectral features between 7.6 and 8.0 eV, the
422 lowest IE reported in the literature for 116 m/z being the one of indene⁹¹.

423
424
425



426

427 **Figure 5: TPES (recorded at 10 eV) and PES of 116 m/z at $HAB = 15$ mm.**

428 **Comparison with a simulated spectrum (in black) corresponding to the sum of reference PES of indene and 1-**
429 **propynylbenzene for a signal ratio of 83:17.**

430

431 Our experimental PES in **fig. 5b** shows a very similar structure to the one reported by Felsmann
432 et al.⁴¹. In this previous work, the 116 m/z signal was also studied with the same setup at SOLEIL,
433 but in a low-pressure, rich flame of cyclopentene ($\phi=1.70$, $p=33.3$ mbar) and using a molecular
434 beam mass spectrometry configuration for the sampling of the species. The PES structure
435 highlights a strong feature in excellent agreement with the IE_{ad} value of 8.14 eV of indene⁷⁶, which
436 allows its clear identification from this spectrum. Concerning 1-propynylbenzene, its lower
437 concentration in comparison with indene combined with the low spectral resolution of the PES

438 make its identification less evident from this spectrum. It is interesting to note that the analysis of
439 this mass is in good agreement with previous similar experiments⁴¹.

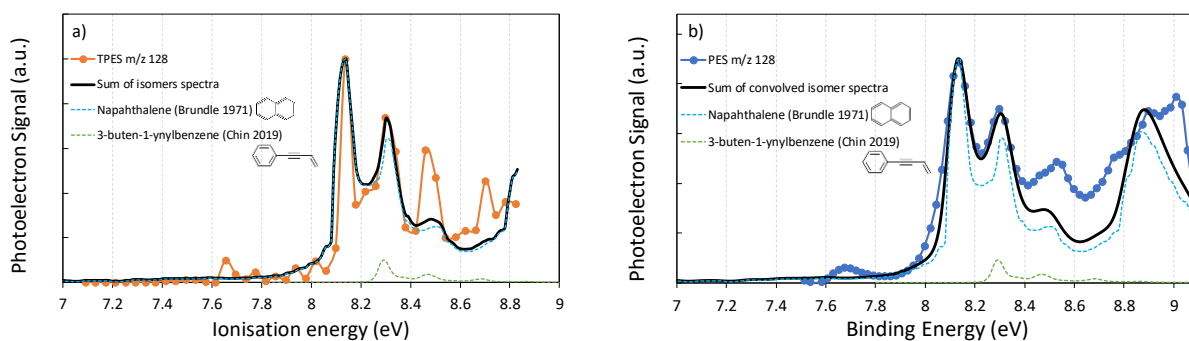
440 Finally, the experimental TPES reported in *fig.5a* shows a much better spectral resolution and
441 agreement with the sum of indene and 1-propynylbenzene spectra. As for the case of 78 *m/z*, we
442 however note some slight differences in this PES/TPES comparison which can mainly be
443 attributed to the degraded SNR of our experiment because of the relatively weak concentration of
444 these species. The mole fraction of indene has been estimated by modeling to be around 0.5 ppm
445 in the flame⁵². Hence, we can state that the TPES allows an accurate identification of indene in
446 this flame while the identification of the signal around 8.40-8.50 eV to 1-propynylbenzene still
447 needs confirmation.

448

449 3.2.3 Analysis of the species at 128 *m/z* ($C_{10}H_8$)

450 TPES and PES measured at HAB = 15 mm and corresponding to 128 *m/z* are reported in *fig. 6*.
451 The PES in *fig. 6b* has been recorded at 10 eV with an acquisition time of 52 minutes, while the
452 TPES in *fig. 6a* required an acquisition time of 4 hours for scanning the ionization energy from
453 7.1 to 9 eV with 0.04 eV steps.

454



455

456 **Figure 6: TPES and PES of 128 *m/z* at HAB=15 mm.**

457 **Comparison with a simulated spectrum (in black) corresponding to the sum of reference PES of naphthalene and**
458 **3-buten-1-ynyl benzene for a signal ratio of 100:10.**

459

460 The TPES shows an intense peak, which is in perfect agreement with the value of the first *IE*
461 potential of naphthalene of 8.14 eV³⁷. Moreover, the experimental spectrum also features a
462 vibrational structure characterized by two other weaker spectral bands peaking around 8.30 and
463 8.50 eV, also in good agreement with the naphthalene reference spectrum⁹². The PES in *fig. 6b*
464 also provides an adequate resolution for the identification of naphthalene sampled from the flame.
465 The first three peaks of the vibrational structure of naphthalene are clearly visible in the PES as
466 well (*fig. 6b*). In addition, the spectrum shows a strong band at 8.85 eV which is also indicative of
467 naphthalene. It should be noted that we again intentionally degraded the resolution of the reference
468 spectrum to match the experimental condition of the PES.

469 In both PES and TPES, two spectral regions of the experimental spectra do not match the
470 reference naphthalene spectrum. The first spectral region is characterized by a weak spectral
471 feature peaking around 7.65 eV for which we could not find any potential candidate with such a
472 low *IE* value. Only azulene, with a first *IE*_{ad} around 7.42 eV, might be responsible for these
473 structures⁹³, but neither its *IE*_{ad} nor its vibronic structure match our spectrum, so that this species
474 can safely be excluded from the list of potential candidates.

475 The second spectral region not perfectly reproduced by the reference spectrum of naphthalene
476 is between 8.4 and 8.7 eV. This part of the spectrum notably displays a significant peak around
477 8.5 eV, which potentially originates from another isomer. Again, we could not find any compound
478 matching this *IE* value. Chin et al.⁹⁴ recently reported simulated PES of some naphthalene isomers
479 from their Franck–Condon calculations. The spectrum reported in green dashed lines in *fig.6*
480 corresponds to the calculated spectrum for 3-buten-1-ynyl benzene. This minor contribution (10%
481 of the naphthalene contribution) improves the fit of the experimental spectra, but is not sufficient
482 to completely explain the shape of the spectrum around 8.5 eV. A shift of the 3-buten-1-ynyl
483 benzene calculated spectrum by a few 100 meV's would improve the correlation with 8.5 eV
484 measured feature in both the PES and TPES.

485 This comparison clearly confirms naphthalene as the main compound at 128 m/z , the mole
486 fraction of which having been previously measured by JCLIF around 1-2 ppm in this region of the
487 flame⁶⁷. The uncertainty on the identification of the potential other minor species highlights the
488 need for reference PES to facilitate the analysis of PAHs formed in sooting flames.

489 To conclude on these first measurements, we can state that the spectral resolution, selectivity
490 and sensitivity of the i^2 PEPICO apparatus enable the selective detection of PAHs structural
491 isomers. The TPES, while requiring longer acquisition times provided a more accurate distinction
492 between structural isomers when reference spectra are available, whereas the faster recorded PES
493 lead to a degraded spectral resolution and lower SNR in comparison with TPES experiments. This
494 can limit their usability for the determination of the contributions of minor species, although they
495 still provide richer information than PIE curves.

496 In the following sections, peaks for larger detected m/z are investigated. The objective of this
497 further work is to reveal the potential formation of CP-PAHs and side-substituted PAHs, likely
498 involved in soot formation, besides the more commonly investigated benzenoid PAHs in the
499 detected species sampled from the nucleation zone of the flame.

500

501 **3.3 Identification of CP-PAHs and side-substituted PAHs in sooting flames**

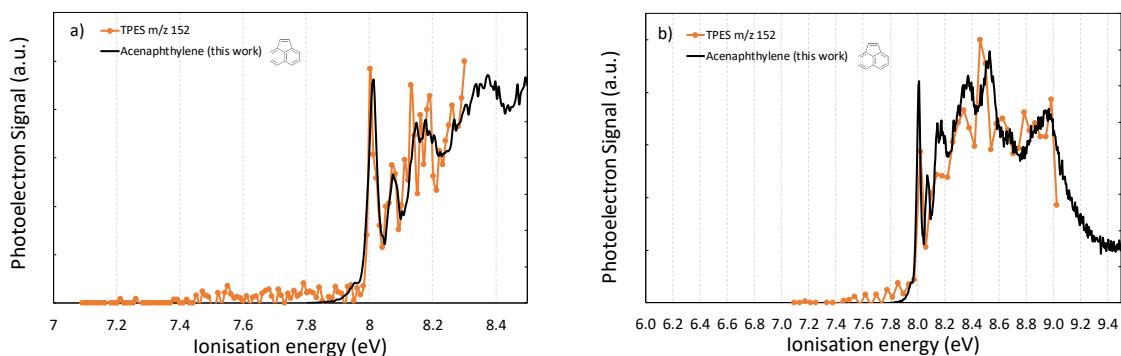
502 To highlight the capabilities of the i^2 PEPICO method for the identification of PAH isomers,
503 further work focused on four detected species usually observed in sooting flames for which
504 structural isomers potentially involving CP-PAHs and side-substituted PAHs might be formed. In
505 the following, we systematically report the TPES recorded at the very beginning of the soot
506 inception zone (HAB = 9 mm), and well inside the flame soot nucleation region (HAB = 15 mm).
507 The corresponding spectra have been determined with different energy steps (0.01 eV at HAB = 9
508 mm and 0.04 eV at HAB = 15 mm, requiring 10 and 4 hours of recording time, respectively).

509

510 **3.3.1 Analysis of the species at 152 m/z ($C_{12}H_8$)**

511 This m/z is frequently detected in the mass spectra of rich and lightly sooting flames. The
512 isomers commonly associated to this mass in the literature are 1-ethylnaphthalene
513 ($IE=8.03$ eV)⁹⁵, 2-ethylnaphthalene ($IE=8.11$ eV)⁹⁵, biphenylene ($IE=7.56$ eV)⁷⁷ and
514 acenaphthylene ($IE=8.02$ eV)⁷⁶. PIE curves are often used for the identification of these species.
515 However, the close ionization threshold values of these compounds do not allow the clear
516 distinction of acenaphthylene and the two ethylnaphthalene isomers.

517 The vibronic structure seen in the TPES reported in *fig.7* provides much more precise
518 information for the identification of these species. *Fig.7a* shows the TPES measured at HAB =
519 9 mm while *fig.7b* shows the spectrum recorded at HAB = 15 mm. The TPES of pure
520 acenaphthylene measured in this work (see *fig.2*) is shown alongside for comparison.
521



522
523 **Figure 7: TPES of 152 m/z at HAB = 9 and 15 mm.**
524 **Comparison with reference TPES of acenaphthylene.**
525

526 Both experiments show an excellent agreement between the TPES recorded in the flame and
527 pure acenaphthylene. The TPES recorded at HAB = 9 mm with a smaller energy step shows
528 vibrational modes clearly assignable to acenaphthylene. The second spectrum measured at
529 HAB = 15 mm, over a broader energy scale but with larger energy steps, does not allow such a
530 detailed analysis because of its lower resolution. However, the first very narrow vibrational mode
531 is still captured by the experiment and the recorded spectrum globally shows an excellent match

532 with the overall shape of the pure acenaphthylene spectrum over this larger energy scale. These
533 data clearly support acenaphthylene as the main species detected at 152 m/z in the nucleation
534 region of the flame.

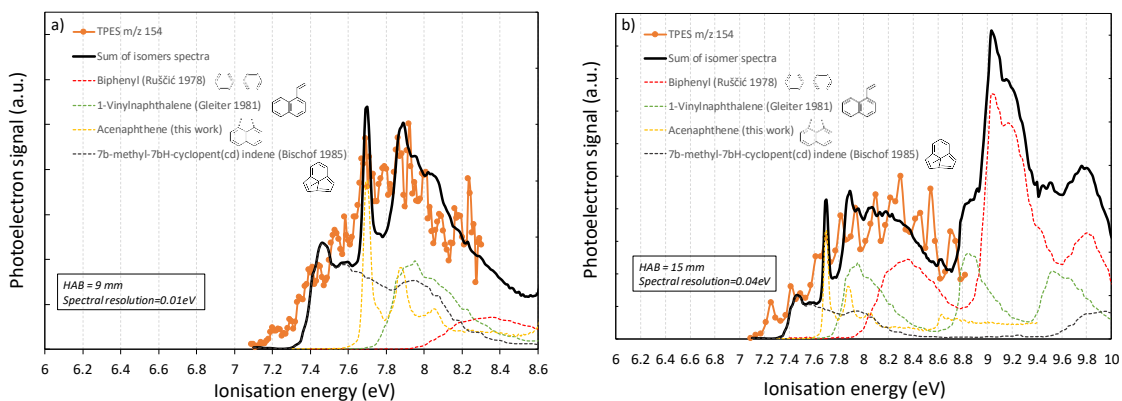
535

536 **3.3.2 Analysis of the species at 154 m/z ($C_{12}H_{10}$)**

537 This mass is usually assigned, in rich flame studies reported the literature, to biphenyl
538 ($IE=8.16$ eV)³⁷ and acenaphthene ($IE=7.67$ eV)³⁷. We have reported in **fig.8a and fig.8b**, the TPES
539 measured at HAB = 9 and 15 mm. These two spectra are relatively noisy in comparison to previous
540 measurements at 152 m/z . Moreover, the global structure of both spectra (HAB = 9 and 15 mm)
541 does not display any specific features as observed for other selected m/z , except a moderate peak
542 around 7.70 eV. The absence of such peculiar spectral features illustrates the limitation of the
543 TPEPICO method which may arise in some cases for the identification of structural isomers.
544 However, these limitations would be even more severe with the use of PIE which would be totally
545 featureless.

546 Hence, to interpret this spectrum, we first tried to reproduce it with a linear combination of the
547 two commonly considered isomers in flames at 154 m/z (biphenyl and acenaphthene) without
548 success, meaning that some additional isomers were to be considered for this mass. However, we
549 note an interesting match between the experimental peak detected around 7.70 eV and the first
550 vibrational mode of the reference spectrum of acenaphthene that we determined (see **Fig.2**). To
551 complete the overall structure of the simulated spectra, we checked in the literature^{37,96} for other
552 species corresponding to this mass, potentially formed in sooting flames.

553



554

555

Figure 8: TPES of 154 m/z at HAB = 9 and 15 mm.

556 **Comparison with a simulated spectrum (in black) corresponding to the sum of reference PES of biphenyl, 1-**
 557 **vinylnaphthalene, acenaphthene and 7b-methyl-7bH-cyclopent(cd)indene for a signal ratio of 26:23:31:20 at**
 558 **9 mm and 57:18:18:7 at 15 mm.**

559

560 Considering all the available spectra in databases^{37,96}, we can only select two species, 1-
 561 vinylnaphthalene ($IE_{\text{vert}}=7.89$ eV) and 7b-methyl-7bH-cyclopent(cd)indene ($IE_{\text{vert}}=7.56$ eV),
 562 potentially matching some of the spectral features experimentally observed in our TPES. Among
 563 these two species, 1-vinylnaphthalene is clearly expected to form in sooting flames according to
 564 the HACA mechanism⁷. 7b-methyl-7bH-cyclopent(cd)indene, to the best of our knowledge, has
 565 never been included in PAH growth models in rich flames. However, it was the only species
 566 proposed in literature possessing a spectral structure peaking around 7.5 eV and thus matching the
 567 first rising shape of the experimental spectrum. 1-vinylnaphthalene, despite being more pertinent
 568 for soot formation and having an IE value estimated around 7.55 eV⁹⁶, could not be considered in
 569 the interpretation of the experimental data since no PES is currently available in the literature.

570 Black spectra reported in **fig.8a** and **8b** correspond to the sum of the different contributions of
 571 the individual spectra of the four considered species. The best matching signal ratio that reproduces
 572 the experimental spectra at respective HAB = 9 and 15 mm are biphenyl (26% and 57%), 1-
 573 vinylnaphthalene (23% and 18%), acenaphthene (31% and 18%), 7b-methyl-7bH-
 574 cyclopent(cd)indene (20% and 7%). However, caution must be exerted regarding the level of

575 confidence in the identification. The most confident information from the comparison reported in
576 *fig. 8a* is the formation of acenaphthene characterized by a very specific peak in the experimental
577 spectrum matching the adiabatic transition of this compound around 7.70 eV and probably also
578 the second peak around 7.85 eV. Conversely, this spectrum does not conclude on the formation of
579 biphenyl at HAB = 9 mm. The main spectral features for this species are indeed located above 9
580 eV, that is slightly off the spectral range of the current experimental spectrum. However, the
581 presence of biphenyl is more likely established on the less resolved TPES spectrum recorded at
582 HAB = 15 mm. As can be seen, biphenyl is the only species with spectral features matching the
583 shape of the spectrum between 8.2 and 8.8 eV. This part of the spectrum strongly evolves between
584 9 to 15 mm and might therefore correspond to the increase of the concentration of biphenyl with
585 HAB. However, it is clear from the simulation that a spectrum registered on a larger spectral
586 energy scale (up to 10 eV) would provide more conclusive information and confidence on the
587 biphenyl formation, as well as having reference PES measured at higher resolution.

588 We can also note that the spectral features of 1-vinylnaphthalene match the experimental
589 spectrum in *fig. 8a* between 7.8 and 8.2 eV. However, this spectral region is relatively large and
590 does not display sufficient specific spectral features to allow a clear distinction of the species.

591 Finally, we have less confidence concerning the formation of 7b-methyl-7bH-
592 cyclopent(cd)indene introduced in our simulated spectrum which appears atypical regarding
593 published chemical analysis of sooting flames. It would have been more interesting to have the
594 PES of 1-vinylnaphthalene which might also match the first spectral features of our TPES and is
595 more expected to be formed in sooting flames.

596 Hence, the analysis for the detected mass 154 m/z , although incomplete, nevertheless
597 highlights the formation of several structural isomers in the nucleation region of the flame. It
598 clearly indicates the formation of acenaphthene and very probably of biphenyl and 1-
599 vinylnaphthalene as well.

600 3.3.3 Analysis of the species at 202 m/z ($C_{16}H_{10}$)

601 202 m/z is usually attributed to pyrene in the analysis of sooting flames carried out by mass
602 spectrometry. Pyrene is considered as a crucial species in soot formation process, and often
603 proposed as a key molecule in the nucleation step leading to the inception of NSPs^{7,52,54,97-99}. In
604 previous works on the same flame^{25,53}, we not only showed the formation of pyrene in the
605 nucleation region of this flame, but also of fluoranthene. Both compounds have been identified by
606 JCLIF²⁵. The mole fractions of pyrene and fluoranthene in this flame have been determined by
607 JCLIF as 0.36 ppm and 0.09 ppm at HAB = 9 mm, respectively, and 0.34 ppm and 0.12 ppm at
608 HAB = 15 mm, respectively²⁵.

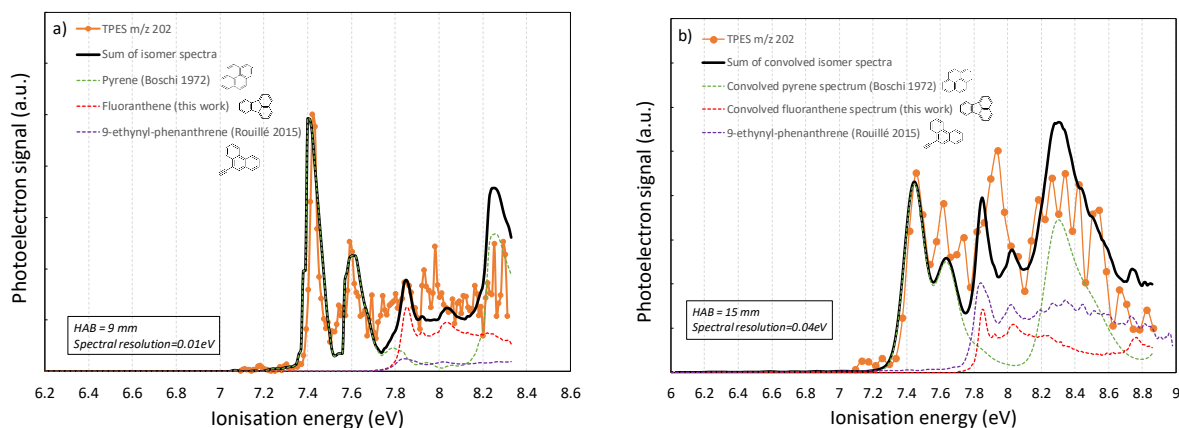
609 Hence, the study of the 202 m/z with the TPES setup is a meaningful benchmark to evaluate its
610 sensitivity in this lightly sooting flame environment. We report in **fig.9** the TPES spectra measured
611 at HAB = 9 and 15 mm with different spectral scan steps. We also report on these figures the
612 calculated spectra (black line) corresponding to the sum of the adjusted contributions of the
613 reference PES of pyrene (green dotted line) measured by Boschi et Schmidt¹⁰⁰ and fluoranthene
614 (red dotted line) measured in this work (see **fig.2**). Moreover, we also considered the 9-
615 ethynylphenanthrene (orange dotted line), also likely to form in this zone. We used for this species
616 the referenced spectrum previously determined by Rouillé et al.⁷⁴.

617 The relative contributions of pyrene and fluoranthene were adjusted for each HAB according
618 to our previous mole fraction measurements in this flame by JCLIF. Based on these data, we
619 obtained $x_{\text{pyrene}}/x_{\text{fluoranthene}}=4$ at HAB = 9 mm and $x_{\text{pyrene}}/x_{\text{fluoranthene}}=3$ at HAB = 15 mm. Finally, we
620 adjusted the contribution of 9-ethynylphenanthrene to get the best agreement between the global
621 simulated spectrum with the experimental one for each HAB. It should be noted that we slightly
622 degraded the resolution of the pyrene and fluoranthene spectra to match the experimental
623 conditions of the spectrum recorded at HAB = 15 mm. Note also that this procedure assumes equal
624 absolute ionization cross-sections for all structural isomers. This assumption is confirmed here by

625 the good agreement obtained when using the mole fractions extracted from JCLIF to match the
626 experimental TPES.

627 The comparison reported in *fig. 9a* provides an excellent agreement between the experimental
628 spectrum and the simulated one obtained by adjusting the intensities of the pyrene and fluoranthene
629 contributions with the value of the corresponding mole fractions determined previously²⁵. This
630 point hence validates the quantitative aspect of the TPES setup, providing experimental spectra
631 with intensities proportional to the concentrations of the measured species.

632 The spectrum in *fig.9a* shows an excellent match of the two first sharp features of the
633 experimental spectrum around 7.43 eV and 7.58 eV with the two first vibrational bands of pyrene
634 PES. These values are in excellent agreement with the *IE* values (7.43 eV and 7.61 eV) of the
635 pyrene reference spectrum¹⁰⁰. This experiment therefore demonstrates that pyrene can be
636 unambiguously identified by its PES measured with the TPES setup at this very low concentration.
637



638

639 **Figure 9: TPES spectra of 202 m/z at HAB = 9 and 15 mm.**

640 **Comparison with a simulated spectrum (in black) corresponding to the sum of reference PES of pyrene,**
641 **fluoranthene and 9-ethynyl-phenanthrene for a signal ratio of 77:19:4 at 9 mm and 56:18:26 at 15 mm.**

642

643 The section of the spectrum above 7.6 eV is noisier but still exhibits a structure that can be
644 reproduced by the weighted sum of the pyrene and fluoranthene referenced PES. We can however

645 note a slight shift between the value of the experimental (7.94 eV) and simulated (7.86 eV) peak,
646 corresponding to the *IE* of the first band of fluoranthene. This difference is attributed to the poor
647 SNR in this zone of the spectrum due to the very weak mole fraction of fluoranthene ($x_{\text{fluoranthene}}$
648 <0.1 ppm), and to the overlap of the spectral contributions of pyrene and fluoranthene. However,
649 the experimental and simulated structures show a satisfying global match allowing the
650 identification of both pyrene and fluoranthene. This comparison also shows a minor contribution
651 of 9-ethynylphenanthrene to the overall spectral structure at HAB = 9 mm. The relative
652 contributions we obtained this way were 77%, 19% and 4% respectively defining the pyrene,
653 fluoranthene and 9-ethynylphenanthrene contributions, although detection of the latter is more
654 speculative since its concentration would then be 0.01 ppm, well below our estimated detection
655 limit.

656 The spectrum recorded at 15 mm exhibits a different structure because of the more important
657 relative contribution of fluoranthene and 9-ethynylphenanthrene in comparison with pyrene in this
658 region of the flame. Again, the contributions of pyrene and fluoranthene have been adjusted on
659 previous JCLIF measurements at this HAB ($x_{\text{pyrene}}/x_{\text{fluoranthene}}=3$), while the relative contribution of
660 9-ethynylphenanthrene has been adjusted to obtain the best fit of the experimental spectrum. The
661 procedure leads to relative ratios of 56%, 18% and 26% for the pyrene, fluoranthene and 9-
662 ethynylphenanthrene contributions, respectively. As seen in Fig. 9b, the experimental spectrum
663 measured at 15 mm can still be correctly reproduced by the contributions of these three species
664 and shows a strong increase of the contribution of the 9-ethynylphenanthrene. However, it would
665 have been difficult to make this statement without the knowledge of the relative contributions of
666 pyrene and fluoranthene deduced from previous JCLIF measurements since fluoranthene and 9-
667 ethynylphenanthrene have very similar spectra in this spectral range. Therefore, to gain confidence
668 in the attribution, acquisition up to 10 eV seems mandatory, as it would allow considering spectral
669 features in a zone with less overlap between the two species.

670 It should be noted that 202 m/z has already been measured in rich or lightly sooting flames
671 studies and generally attributed to pyrene alone^{31,82} by the analysis of the PIE curves. However, in
672 two recent papers, Johansson et al.^{35,101} reported experimental PIE curves of 202 m/z obtained from
673 condensed species onto incipient soot particles and sampled from different ethylene flames. In
674 these works, they concluded that their PIE curves could not be attributed to pyrene alone, and that
675 the contribution of fluoranthene had also to be considered. Here, we reach the same conclusion for
676 the gas phase. Interestingly, the adjusted contribution of these two PAHs (66% and 33%)
677 determined by Johansson et al.³⁵ for the condensed species of 202 m/z onto incipient soot particles
678 is very similar to this work. This similarity is remarkable, considering the differences between
679 these two flame setups (atmospheric pressure ethylene flame vs. low pressure methane flame).

680 Hence, TPES data confirm the formation of fluoranthene (and probably 9-ethynylphenanthrene)
681 in addition to pyrene at 202 m/z , and highlights their potential implication in the soot nucleation
682 process, further reinforced by their presence as condensates onto incipient soot particles^{35,101}.

683

684 **3.3.4 Analysis of the species at 226 m/z ($C_{18}H_{10}$)**

685 226 m/z is often attributed to CP-PAHs likely involved in the soot nucleation process^{11,12,101}.
686 However, only a few analyses are reported in the literature and no clear attribution has ever been
687 reported before. Several factors can explain the difficulty to analyze 226 m/z as the large number
688 of potential structural isomers and the lack of reference data such as *IE*, PIE curves or PES. To
689 date, only five out of the whole possible structural isomers are listed in the online NIST database³⁷,
690 that furthermore only contains incomplete information: benzo[ghi]fluoranthene ,
691 cyclopenta[cd]-pyrene , cyclopent[fg]aceanthrylene 3,4-dihydrocyclopenta[cd]pyrene ,
692 and benz[mno]aceanthrylene . It is worth noting that all these candidates are CP-PAHs
693 containing a five-carbon ring in their structures. This lack of data makes therefore the interpretation

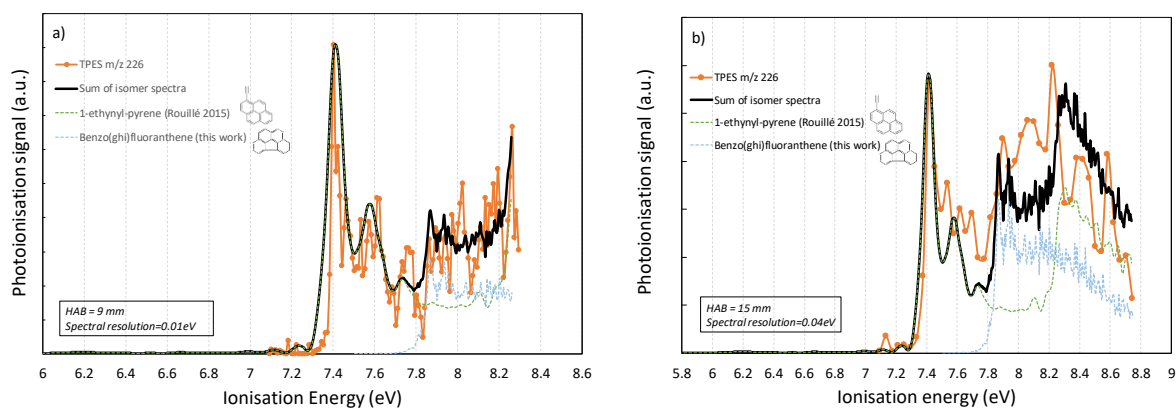
694 of 226 m/z PES/TPES a very challenging task. In this work, we determined for the first time, the
695 TPES spectra of the benzo[ghi]fluoranthene to aid in the analysis of this peak. Among the other

696 potential candidates, we also considered the 1-ethynyl-pyrene C#Cc1ccc2ccc3ccccc3cc2c1, the spectrum of which has
697 been recorded by Rouillé et al.⁷⁴

698 As for previous mass analyses, we report in **fig.10** the TPES corresponding to 226 m/z measured
699 with different spectral resolutions and over different energy ranges at HAB = 9 and 15 mm
700 compared to the simulated spectrum obtained with the reference spectra of 1-ethynyl-pyrene and
701 benzo(ghi)fluoranthene.

702

703



704

705

Figure 10: TPES of 226 m/z at HAB = 9 and 15 mm.

706 *Comparison with a simulated spectrum (in black) corresponding to the sum of reference PES of 1-ethynyl-pyrene*
707 *and benzo(ghi)fluoranthene for a signal ratio of 77:23 at 9 mm and 65:35 at 15 mm.*

708

709 As seen in **fig. 10a**, the experimental and simulated spectra are in excellent agreement by
710 considering only 1-ethynyl-pyrene and benzo(ghi)fluoranthene. An excellent match of the two first
711 peaks of the experimental structure with the first two vibrational bands of 1-ethynyl-pyrene,
712 peaking at 7.41 and 7.58 eV, is observed. The second part of the spectrum is noisier but also shows
713 an excellent agreement with the adjusted contributions of both 1-ethynyl-pyrene and

714 benzo(ghi)fluoranthene. We reached the best agreement by adjusting the relative signal
715 contribution of 1-ethynyl-pyrene and benzo(ghi)fluoranthene equal to 77% and 23%. The
716 spectrum recorded at HAB = 15 mm over a larger energy range still provides an adequate spectral
717 resolution to identify these two species. The first peak of the spectrum is notably in perfect
718 agreement with the energy of the first vibrational band of 1-ethynyl-pyrene. The rest of the
719 spectrum is globally correctly reproduced by the simulated structure by considering relative
720 contributions of 1-ethynyl-pyrene and benzo(ghi)fluoranthene equal to 65% and 35%. These data
721 show again that CP-PAH and substituted PAHs actively occur in the nucleation region of the
722 flame.

723 Recently, Adamson et al.¹⁰² reported experiments, carried out with a tandem mass spectrometer,
724 showing the formation of aliphatically bridged structures in an ethylene/O₂ coflow diffusion flame.
725 These structures, constituted of PAHs bonded by a carbon chain, are suggested as a particle seeds
726 in sooting flames. Their formation would be based on a growth mechanism involving side-
727 substituted aromatics formed through reactions of smaller aromatic species and aliphatic
728 hydrocarbons. In this work, Adamson et al.¹⁰² notably detected the species C₁₈H₁₀ at 226 *m/z* as a
729 very stable building block. The information provided in this work in the nucleation zone,
730 complementary highlights the formation of a side-substituted PAH as part of the compounds
731 detected at this mass and therefore their possible involvement in the formation of such
732 aliphatically-bridged PAHs. Furthermore, recent studies suggested that these compounds would
733 be stable enough to resist in flame conditions¹⁰³ and might be at the origin of the broadband
734 fluorescence emission spectra commonly observed in such sooting flames by laser excitation^{23,104}
735 in the nucleation zone.

736

737

738

739 4 Conclusion

740 This work demonstrates and benchmarks the capabilities of the multiplex i^2 PEPICO technique
741 to study sooting flames. Mass-selected PES and TPES spectra corresponding to different PAHs
742 have been reported for samples obtained at different heights above the burner in a sooting low-
743 pressure methane flame. The identification of structural isomers at each m/z channel relies on the
744 comparison of the recorded experimental spectra with reference PES, which act as molecular
745 fingerprints. From this work, it appears that the analysis of the TPES spectra enables the accurate
746 identification of the PAHs formed in the flame. The PES, which are recorded at fixed photon
747 energies with much shorter acquisition time than TPES scans, present a less accurate resolution
748 and lower SNR. However, these spectra have been shown for the smallest species, at least up to
749 naphthalene, to be sufficiently resolved to capture the main electronic features of the PAHs and in
750 some cases, even the vibrational progressions. However, for the largest PAHs with concentrations
751 below the ppm, we observed that only the TPES approach provided sufficient sensitivity and
752 spectral selectivity to enable the identification of the different structural isomers.

753 This study provides evidence of the formation of CP-PAHs in the nucleation zone of the
754 sooting flame, such as indene, acenaphthylene, fluoranthene and benzo(ghi)fluoranthene. Such
755 CP-PAHs likely correspond to the cyclopentaring observed in the curved graphene layer present
756 in the core region of soot particles⁵⁵. Moreover, we also highlight the presence of side-substituted
757 aromatics besides CP-PAHs which have been recently suggested to lead to the formation of
758 aliphatically bridged structures which could serve as a particle seed¹⁰². This work emphasizes the
759 importance of considering the chemical pathways and overall kinetics leading to the formation of
760 CP-PAHs and side-substituted aromatics in the development of soot formation mechanisms⁵⁷.

761 This first attempt of using the PEPICO setup of the DESIRS beamline at SOLEIL for the study
762 of low pressure sooting premixed flames therefore appears very encouraging and shows a high
763 potential for understanding in situ the mechanisms of soot and PAHs formation in laboratory

764 flames. Means of improvement include the recording of higher quality PES to feed the current
765 database—to which this work has already contributed with the reporting of the PES of
766 acenaphthene, acenaphthylene, fluoranthene and benzo(ghi)fluoranthene—or the challenging
767 measurement or calculation of absolute cross-sections to increase the quantitative potential of this
768 method. The sensitivity of the setup, although adequate, might be improved to provide a better
769 identification of PAH isomers by increasing the molecular beam density in the ionization region
770 (shortening the nozzle-synchrotron beam distance, improving the gas inlet). However, we showed
771 that the capabilities of the current setup already enable the possibility of more systematic studies
772 aiming at the determination of experimental profiles of moderate size PAHs isomers involved in
773 the soot formation process in flames. A deeper understanding of the soot nucleation process will
774 require, at some point in the future, extending the measurements shown in this paper to the
775 particulate phase at the very beginning of the soot formation. In this context, the use of the
776 SAPHIRS chamber dedicated aerodynamic lens system, coupled to a thermodesorbing tip, could
777 enable the measurements of the detailed chemical composition of nascent soot particles⁴⁶.

778

779 **Acknowledgements**

780 This work is a contribution to the labex CAPPa and the CPER research project CLIMIBIO. The
781 authors thank the French Ministère de l'Enseignement Supérieur et de la Recherche, the Hauts de
782 France Region and the European Funds for Regional Economical Development for their financial
783 support to this project." We are grateful to J.-F. Gil for his technical help around the SAPHIRS
784 set-up. We warmly thank the whole SOLEIL staff for running the facility and providing beamtime
785 under project number 20151078 and 20170070.

786

787

788

- 790 1 J. C. Chow, Health Effects of Fine Particulate Air Pollution: Lines that Connect, *Journal of*
791 *the Air & Waste Management Association*, 2006, **56**, 707–708.
- 792 2 T. Petry, P. Schmid and C. Schlatter, The use of toxic equivalency factors in assessing
793 occupational and environmental health risk associated with exposure to airborne mixtures of
794 polycyclic aromatic hydrocarbons (PAHs), *Chemosphere*, 1996, **32**, 639–648.
- 795 3 R. Niranjana and A. K. Thakur, The Toxicological Mechanisms of Environmental Soot (Black
796 Carbon) and Carbon Black: Focus on Oxidative Stress and Inflammatory Pathways, *Front.*
797 *Immunol.*, , DOI:10.3389/fimmu.2017.00763.
- 798 4 S. S. Lim, T. Vos, A. D. Flaxman, G. Danaei, K. Shibuya, H. Adair-Rohani, M. A. AlMazroa,
799 M. Amann, H. R. Anderson, K. G. Andrews, M. Aryee, C. Atkinson, L. J. Bacchus, A. N.
800 Bahalim, K. Balakrishnan, J. Balmes, S. Barker-Collo, A. Baxter, M. L. Bell, J. D. Blore, F.
801 Blyth, C. Bonner, G. Borges, R. Bourne, M. Boussinesq, M. Brauer, P. Brooks, N. G. Bruce,
802 B. Brunekreef, C. Bryan-Hancock, C. Bucello, R. Buchbinder, F. Bull, R. T. Burnett, T. E.
803 Byers, B. Calabria, J. Carapetis, E. Carnahan, Z. Chafe, F. Charlson, H. Chen, J. S. Chen, A.
804 T.-A. Cheng, J. C. Child, A. Cohen, K. E. Colson, B. C. Cowie, S. Darby, S. Darling, A.
805 Davis, L. Degenhardt, F. Dentener, D. C. Des Jarlais, K. Devries, M. Dherani, E. L. Ding, E.
806 R. Dorsey, T. Driscoll, K. Edmond, S. E. Ali, R. E. Engell, P. J. Erwin, S. Fahimi, G. Falder,
807 F. Farzadfar, A. Ferrari, M. M. Finucane, S. Flaxman, F. G. R. Fowkes, G. Freedman, M. K.
808 Freeman, E. Gakidou, S. Ghosh, E. Giovannucci, G. Gmel, K. Graham, R. Grainger, B. Grant,
809 D. Gunnell, H. R. Gutierrez, W. Hall, H. W. Hoek, A. Hogan, H. D. Hosgood, D. Hoy, H. Hu,
810 B. J. Hubbell, S. J. Hutchings, S. E. Ibeanusi, G. L. Jacklyn, R. Jasrasaria, J. B. Jonas, H. Kan,
811 J. A. Kanis, N. Kassebaum, N. Kawakami, Y.-H. Khang, S. Khatibzadeh, J.-P. Khoo, C. Kok,
812 F. Laden, R. Lalloo, Q. Lan, T. Lathlean, J. L. Leasher, J. Leigh, Y. Li, J. K. Lin, S. E.
813 Lipshultz, S. London, R. Lozano, Y. Lu, J. Mak, R. Malekzadeh, L. Mallinger, W. Marcenes,
814 L. March, R. Marks, R. Martin, P. McGale, J. McGrath, S. Mehta, Z. A. Memish, G. A.
815 Mensah, T. R. Merriman, R. Micha, C. Michaud, V. Mishra, K. M. Hanafiah, A. A. Mokdad,
816 L. Morawska, D. Mozaffarian, T. Murphy, M. Naghavi, B. Neal, P. K. Nelson, J. M. Nolla, R.
817 Norman, C. Olives, S. B. Omer, J. Orchard, R. Osborne, B. Ostro, A. Page, K. D. Pandey, C.
818 D. Parry, E. Passmore, J. Patra, N. Pearce, P. M. Pelizzari, M. Petzold, M. R. Phillips, D.
819 Pope, C. A. Pope, J. Powles, M. Rao, H. Razavi, E. A. Rehfuss, J. T. Rehm, B. Ritz, F. P.
820 Rivara, T. Roberts, C. Robinson, J. A. Rodriguez-Portales, I. Romieu, R. Room, L. C.
821 Rosenfeld, A. Roy, L. Rushton, J. A. Salomon, U. Sampson, L. Sanchez-Riera, E. Sanman, A.
822 Sapkota, S. Seedat, P. Shi, K. Shield, R. Shivakoti, G. M. Singh, D. A. Sleet, E. Smith, K. R.
823 Smith, N. J. Stapelberg, K. Steenland, H. Stöckl, L. J. Stovner, K. Straif, L. Straney, G. D.
824 Thurston, J. H. Tran, R. Van Dingenen, A. van Donkelaar, J. L. Veerman, L. Vijayakumar, R.
825 Weintraub, M. M. Weissman, R. A. White, H. Whiteford, S. T. Wiersma, J. D. Wilkinson, H.
826 C. Williams, W. Williams, N. Wilson, A. D. Woolf, P. Yip, J. M. Zielinski, A. D. Lopez, C. J.
827 Murray and M. Ezzati, A comparative risk assessment of burden of disease and injury
828 attributable to 67 risk factors and risk factor clusters in 21 regions, 1990–2010: a systematic
829 analysis for the Global Burden of Disease Study 2010, *The Lancet*, 2012, **380**, 2224–2260.
- 830 5 T. C. Bond, S. J. Doherty, D. W. Fahey, P. M. Forster, T. Berntsen, B. J. DeAngelo, M. G.
831 Flanner, S. Ghan, B. Kärcher, D. Koch, S. Kinne, Y. Kondo, P. K. Quinn, M. C. Sarofim, M.
832 G. Schultz, M. Schulz, C. Venkataraman, H. Zhang, S. Zhang, N. Bellouin, S. K. Guttikunda,
833 P. K. Hopke, M. Z. Jacobson, J. W. Kaiser, Z. Klimont, U. Lohmann, J. P. Schwarz, D.
834 Shindell, T. Storelvmo, S. G. Warren and C. S. Zender, Bounding the role of black carbon in
835 the climate system: A scientific assessment, *Journal of Geophysical Research: Atmospheres*,
836 2013, **118**, 5380–5552.

- 837 6 B. Gorbunov, A. Baklanov, N. Kakutkina, H. L. Windsor and R. Toumi, Ice nucleation on
838 soot particles, *Journal of Aerosol Science*, 2001, **32**, 199–215.
- 839 7 M. Frenklach and H. Wang, Detailed modeling of soot particle nucleation and growth,
840 *Symposium (International) on Combustion*, 1991, **23**, 1559–1566.
- 841 8 A. D’Anna, *Combustion Generated Fine Carbonaceous Particles*, KIT Scientific Publishing,
842 Karlsruhe, 2009.
- 843 9 A. D’Anna, Combustion-formed nanoparticles, *Proceedings of the Combustion Institute*,
844 2009, **32**, 593–613.
- 845 10 H. Wang, Formation of nascent soot and other condensed-phase materials in flames,
846 *Proceedings of the Combustion Institute*, 2011, **33**, 41–67.
- 847 11 B. Shukla and M. Koshi, A novel route for PAH growth in HACA based mechanisms,
848 *Combustion and Flame*, 2012, **159**, 3589–3596.
- 849 12 B. Shukla and M. Koshi, Comparative study on the growth mechanisms of PAHs, *Combustion*
850 *and Flame*, 2011, **158**, 369–375.
- 851 13 C. S. McEnally, L. D. Pfefferle, B. Atakan and K. Kohse-Höinghaus, Studies of aromatic
852 hydrocarbon formation mechanisms in flames: Progress towards closing the fuel gap,
853 *Progress in Energy and Combustion Science*, 2006, **32**, 247–294.
- 854 14 M. Commodo, K. Kaiser, G. De Falco, P. Minutolo, F. Schulz, A. D’Anna and L. Gross, On
855 the early stages of soot formation: Molecular structure elucidation by high-resolution atomic
856 force microscopy, *Combustion and Flame*, 2019, **205**, 154–164.
- 857 15 K. Siegmann and K. Sattler, Formation mechanism for polycyclic aromatic hydrocarbons in
858 methane flames, *J. Chem. Phys.*, 1999, **112**, 698–709.
- 859 16 J. Xiao, E. Austin and W. L. Roberts, Relative Polycyclic Aromatic Hydrocarbon
860 Concentrations in Unsteady Counterflow Diffusion Flames, *Combustion Science and*
861 *Technology*, 2005, **177**, 691–713.
- 862 17 S. Bejaoui, X. Mercier, P. Desgroux and E. Therssen, Laser induced fluorescence
863 spectroscopy of aromatic species produced in atmospheric sooting flames using UV and
864 visible excitation wavelengths, *Combustion and Flame*, 2014, **161**, 2479–2491.
- 865 18 K. C. Smyth, C. R. Shaddix and D. A. Everest, Aspects of soot dynamics as revealed by
866 measurements of broadband fluorescence and flame luminosity in flickering diffusion flames,
867 *Combustion and Flame*, 1997, **111**, 185–207.
- 868 19 S.-Y. Lee, S. R. Turns and R. J. Santoro, Measurements of soot, OH, and PAH concentrations
869 in turbulent ethylene/air jet flames, *Combustion and Flame*, 2009, **156**, 2264–2275.
- 870 20 M. Köhler, K. P. Geigle, T. Blacha, P. Gerlinger and W. Meier, Experimental characterization
871 and numerical simulation of a sooting lifted turbulent jet diffusion flame, *Combustion and*
872 *Flame*, 2012, **159**, 2620–2635.
- 873 21 A. Ciajolo, R. Ragucci, B. Apicella, R. Barbella, M. de Joannon and A. Tregrossi,
874 Fluorescence spectroscopy of aromatic species produced in rich premixed ethylene flames,
875 *Chemosphere*, 2001, **42**, 835–841.
- 876 22 M. Sirignano, A. Collina, M. Commodo, P. Minutolo and A. D’Anna, Detection of aromatic
877 hydrocarbons and incipient particles in an opposed-flow flame of ethylene by spectral and
878 time-resolved laser induced emission spectroscopy, *Combustion and Flame*, 2012, **159**, 1663–
879 1669.
- 880 23 X. Mercier, O. Carrivain, C. Irimiea, A. Faccinetto and E. Therssen, Dimers of polycyclic
881 aromatic hydrocarbons: the missing pieces in the soot formation process, *Phys. Chem. Chem.*
882 *Phys.*, 2019, **21**, 8282–8294.
- 883 24 Y. Zhang, Y. Li, L. Wang, P. Liu, R. Zhan, Z. Huang and H. Lin, Investigation on the LIF
884 spectrum superposition of gas-phase PAH mixtures at elevated temperatures: potential for the
885 analysis of PAH LIF spectra in sooting flames, *Appl. Phys. B*, 2019, **125**, 72.

- 886 25 T. Mouton, X. Mercier and P. Desgroux, Isomer discrimination of PAHs formed in sooting
887 flames by jet-cooled laser-induced fluorescence: application to the measurement of pyrene
888 and fluoranthene, *Applied Physics B*, 2016, **122**, 123–139.
- 889 26 X. Mercier, M. Wartel, J.-F. Pauwels and P. Desgroux, Implementation of a new
890 spectroscopic method to quantify aromatic species involved in the formation of soot particles
891 in flames, *Applied Physics B: Lasers and Optics*, 2008, **91**, 387–395.
- 892 27 C. A. Taatjes, N. Hansen, D. L. Osborn, K. Kohse-Hoinghaus, T. A. Cool and P. R.
893 Westmoreland, “Imaging” combustion chemistry via multiplexed synchrotron-photoionization
894 mass spectrometry, *Physical Chemistry Chemical Physics*, 2008, **10**, 20–34.
- 895 28 F. Qi, R. Yang, B. Yang, C. Huang, L. Wei, J. Wang, L. Sheng and Y. Zhang, Isomeric
896 identification of polycyclic aromatic hydrocarbons formed in combustion with tunable
897 vacuum ultraviolet photoionization, *Review of Scientific Instruments*, 2006, **77**, 084101.
- 898 29 L. Zhao, R. I. Kaiser, B. Xu, U. Ablikim, M. Ahmed, D. Joshi, G. Veber, F. R. Fischer and A.
899 M. Mebel, Pyrene synthesis in circumstellar envelopes and its role in the formation of 2D
900 nanostructures, 2018, **2**, 413–419.
- 901 30 F. Qi, Combustion Chemistry Probed by Synchrotron VUV Photo-ionization Mass
902 Spectrometry, *Proceedings of the Combustion Institute*, 2013, **34**, 33–63.
- 903 31 Y. Li, L. Zhang, Z. Tian, T. Yuan, J. Wang, B. Yang and F. Qi, Experimental Study of a Fuel-
904 Rich Premixed Toluene Flame at Low Pressure, *Energy Fuels*, 2009, **23**, 1473–1485.
- 905 32 Y. Li, Z. Tian, L. Zhang, T. Yuan, K. Zhang, B. Yang and F. Qi, An experimental study of the
906 rich premixed ethylbenzene flame at low pressure, *Proceedings of the Combustion Institute*,
907 2009, **32**, 647–655.
- 908 33 Y. Li, L. Zhang, Z. Tian, T. Yuan, K. Zhang, B. Yang and F. Qi, Investigation of the rich
909 premixed laminar acetylene/oxygen/argon flame: Comprehensive flame structure and special
910 concerns of polyynes, *Proceedings of the Combustion Institute*, 2009, **32**, 1293–1300.
- 911 34 B. Yang, Y. Li, L. Wei, C. Huang, J. Wang, Z. Tian, R. Yang, L. Sheng, Y. Zhang and F. Qi,
912 An experimental study of the premixed benzene/oxygen/argon flame with tunable synchrotron
913 photoionization, *Proceedings of the Combustion Institute*, 2007, **31**, 555–563.
- 914 35 K. O. Johansson, J. Zádor, P. Elvati, M. F. Campbell, P. E. Schrader, N. K. Richards-
915 Henderson, K. R. Wilson, A. Violi and H. A. Michelsen, Critical Assessment of
916 Photoionization Efficiency Measurements for Characterization of Soot-Precursor Species, *J.*
917 *Phys. Chem. A*, 2017, **121**, 4475–4485.
- 918 36 T. Zhang, L. Zhang, X. Hong, K. Zhang, F. Qi, C. K. Law, T. Ye, P. Zhao and Y. Chen, An
919 experimental and theoretical study of toluene pyrolysis with tunable synchrotron VUV
920 photoionization and molecular-beam mass spectrometry, *Combustion and Flame*, 2009, **156**,
921 2071–2083.
- 922 37 S. G. Lias, in *NIST Chemistry WebBook, NIST Standard Reference Database Number 69*,
923 *edited by P. J. Linstrom and W. G. Mallard (National Institute of Standards and Technology,*
924 *Gaithersburg, MD), 20899. <http://webbook.nist.gov/chemistry/>. Accessed 26 November 2012,*
925 2012.
- 926 38 P. Bréchnignac, G. A. Garcia, C. Falvo, C. Joblin, D. Kokkin, A. Bonnamy, P. Parneix, T.
927 Pino, O. Pirali, G. Mulas and L. Nahon, Photoionization of cold gas phase coronene and its
928 clusters: Autoionization resonances in monomer, dimer, and trimer and electronic structure of
929 monomer cation, *J. Chem. Phys.*, 2014, **141**, 164325.
- 930 39 P. Oßwald, P. Hemberger, T. Bierkandt, E. Akyildiz, M. Köhler, A. Bodi, T. Gerber and T.
931 Kasper, In situ flame chemistry tracing by imaging photoelectron photoion coincidence
932 spectroscopy, *Review of Scientific Instruments*, 2014, **85**, 025101.
- 933 40 D. Felsmann, K. Moshhammer, J. Krüger, A. Lackner, A. Brockhinke, T. Kasper, T. Bierkandt,
934 E. Akyildiz, N. Hansen, A. Lucassen, P. Oßwald, M. Köhler, G. A. Garcia, L. Nahon, P.
935 Hemberger, A. Bodi, T. Gerber and K. Kohse-Höinghaus, Electron ionization, photoionization

- 936 and photoelectron/photoion coincidence spectroscopy in mass-spectrometric investigations of
937 a low-pressure ethylene/oxygen flame, *Proceedings of the Combustion Institute*, 2015, **35**,
938 779–786.
- 939 41 D. Felsmann, A. Lucassen, J. Krüger, C. Hemken, L.-S. Tran, J. Pieper, G. A. Garcia, A.
940 Brockhinke, L. Nahon and K. Kohse-Höinghaus, Progress in Fixed-Photon-Energy Time-
941 Efficient Double Imaging Photoelectron/Photoion Coincidence Measurements in Quantitative
942 Flame Analysis, *Zeitschrift für Physikalische Chemie*, 2016, **230**, 1067–1097.
- 943 42 J. Pieper, S. Schmitt, C. Hemken, E. Davies, J. Wullenkord, A. Brockhinke, J. Krüger, G. A.
944 Garcia, L. Nahon, A. Lucassen, W. Eisfeld and K. Kohse-Höinghaus, Isomer Identification in
945 Flames with Double-Imaging Photoelectron/Photoion Coincidence Spectroscopy (i2PEPICO)
946 using Measured and Calculated Reference Photoelectron Spectra, *Zeitschrift für Physikalische
947 Chemie*, 2018, **232**, 153–187.
- 948 43 J. Krüger, G. A. Garcia, D. Felsmann, K. Moshhammer, A. Lackner, A. Brockhinke, L. Nahon
949 and K. Kohse-Höinghaus, Photoelectron–photoion coincidence spectroscopy for multiplexed
950 detection of intermediate species in a flame, *Phys. Chem. Chem. Phys.*, 2014, **16**, 22791–
951 22804.
- 952 44 P. Hemberger, V. B. F. Custodis, A. Bodi, T. Gerber and J. A. van Bokhoven, Understanding
953 the mechanism of catalytic fast pyrolysis by unveiling reactive intermediates in heterogeneous
954 catalysis, *Nat Commun*, 2017, **8**, 1–9.
- 955 45 D. Krüger, P. Oßwald, M. Köhler, P. Hemberger, T. Bierkandt, Y. Karakaya and T. Kasper,
956 Hydrogen abstraction ratios: A systematic iPEPICO spectroscopic investigation in laminar
957 flames, *Combustion and Flame*, 2018, **191**, 343–352.
- 958 46 M. T. Baeza-Romero, F. Gaie-Levrel, A. Mahjoub, V. López-Arza, G. A. Garcia and L.
959 Nahon, A smog chamber study coupling a photoionization aerosol electron/ion spectrometer
960 to VUV synchrotron radiation: organic and inorganic-organic mixed aerosol analysis, *Eur.
961 Phys. J. D*, 2016, **70**, 154.
- 962 47 J. Bourgalais, Z. Gouid, O. Herbinet, G. A. Garcia, P. Arnoux, Z. Wang, L.-S. Tran, G.
963 Vanhove, M. Hochlaf, L. Nahon and F. Battin-Leclerc, Isomer-sensitive characterization of
964 low temperature oxidation reaction products by coupling a jet-stirred reactor to an electron/ion
965 coincidence spectrometer: case of n-pentane, *Phys. Chem. Chem. Phys.*, 2020, **22**, 1222–1241.
- 966 48 A. Bodi, P. Hemberger, D. L. Osborn and B. Sztáray, Mass-Resolved Isomer-Selective
967 Chemical Analysis with Imaging Photoelectron Photoion Coincidence Spectroscopy, *J. Phys.
968 Chem. Lett.*, 2013, **4**, 2948–2952.
- 969 49 M. Wartel, J.-F. Pauwels, P. Desgroux and X. Mercier, Pyrene Measurements in Sooting Low
970 Pressure Methane Flames by Jet-Cooled Laser-Induced Fluorescence, *Journal of Physical
971 Chemistry A*, 2011, **115**, 14153–14162.
- 972 50 H. Bladh, N.-E. Olofsson, T. Mouton, J. Simonsson, X. Mercier, A. Faccinnetto, P.-E.
973 Bengtsson and P. Desgroux, Probing the smallest soot particles in low-sooting premixed
974 flames using laser-induced incandescence, *Proceedings of the Combustion Institute*, 2015, **35**,
975 1843–1850.
- 976 51 T. Mouton, X. Mercier, M. Wartel, N. Lamoureux and P. Desgroux, Laser-induced
977 incandescence technique to identify soot nucleation and very small particles in low-pressure
978 methane flames, *Applied Physics B: Lasers and Optics*, 2013, **112**, 369–379.
- 979 52 A. El Bakali, X. Mercier, M. Wartel, F. Acevedo, I. S. Burns, L. Gasnot, J.-F. Pauwels and P.
980 Desgroux, Modeling of PAHs in low pressure sooting premixed methane flame, *Energy*,
981 2012, **43**, 73–84.
- 982 53 P. Desgroux, A. Faccinnetto, X. Mercier, T. Mouton, D. Aubagnac Karkar and A. El Bakali,
983 Comparative study of the soot formation process in a “nucleation” and a “sooting” low
984 pressure premixed methane flame, *Combustion and Flame*, 2017, **184**, 153–166.

- 985 54D. Aubagnac-Karkar, A. El Bakali and P. Desgroux, Soot particles inception and PAH
 986 condensation modelling applied in a soot model utilizing a sectional method, *Combustion and*
 987 *Flame*, 2018, **189**, 190–206.
- 988 55J.-O. Müller, D. S. Su, U. Wild and R. Schlögl, Bulk and surface structural investigations of
 989 diesel engine soot and carbon black, *Phys. Chem. Chem. Phys.*, 2007, **9**, 4018–4025.
- 990 56M. Wei, T. Zhang, X. Chen, F. Yan, G. Guo and D. Zhang, Formation of bicyclic polycyclic
 991 aromatic hydrocarbons (PAHs) from the reaction of a phenyl radical with cis-3-penten-1-yne,
 992 *RSC Adv.*, 2018, **8**, 13226–13236.
- 993 57M. Frenklach and A. M. Mebel, On the mechanism of soot nucleation, *Phys. Chem. Chem.*
 994 *Phys.*, 2020, **22**, 5314–5331.
- 995 58R. A. Krueger and G. Blanquart, Predicting the photoresponse of soot nuclei: Spectroscopic
 996 characteristics of aromatic aggregates containing five-membered rings, *Combustion and*
 997 *Flame*, 2020, **217**, 85–92.
- 998 59M. Tia, B. Cunha de Miranda, S. Daly, F. Gaie-Levrel, G. A. Garcia, I. Powis and L. Nahon,
 999 Chiral Asymmetry in the Photoionization of Gas-Phase Amino-Acid Alanine at Lyman- α
 1000 Radiation Wavelength, *J. Phys. Chem. Lett.*, 2013, **4**, 2698–2704.
- 1001 60X. Tang, G. A. Garcia, J.-F. Gil and L. Nahon, Vacuum upgrade and enhanced performances
 1002 of the double imaging electron/ion coincidence end-station at the vacuum ultraviolet beamline
 1003 DESIRS, *Review of Scientific Instruments*, 2015, **86**, 123108.
- 1004 61L. Nahon, N. de Oliveira, G. A. Garcia, J.-F. Gil, B. Pilette, O. Marcouillé, B. Lagarde and F.
 1005 Polack, DESIRS: a state-of-the-art VUV beamline featuring high resolution and variable
 1006 polarization for spectroscopy and dichroism at SOLEIL, *J Synchrotron Rad*, 2012, **19**, 508–
 1007 520.
- 1008 62B. Mercier, M. Compin, C. Prevost, G. Bellec, R. Thissen, O. Dutuit and L. Nahon,
 1009 Experimental and theoretical study of a differentially pumped absorption gas cell used as a
 1010 low energy-pass filter in the vacuum ultraviolet photon energy range, *Journal of Vacuum*
 1011 *Science & Technology A*, 2000, **18**, 2533–2541.
- 1012 63K. Yoshino and Y. Tanaka, Absorption spectrum of krypton in the vacuum uv region, *J. Opt.*
 1013 *Soc. Am., JOS A*, 1979, **69**, 159–165.
- 1014 64G. A. Garcia, B. K. Cunha de Miranda, M. Tia, S. Daly and L. Nahon, DELICIOUS III: a
 1015 multipurpose double imaging particle coincidence spectrometer for gas phase vacuum
 1016 ultraviolet photodynamics studies, *Rev Sci Instrum*, 2013, **84**, 053112.
- 1017 65G. A. Garcia, X. Tang, J.-F. Gil, L. Nahon, M. Ward, S. Batut, C. Fittschen, C. A. Taatjes, D.
 1018 L. Osborn and J.-C. Loison, Synchrotron-based double imaging photoelectron/photoion
 1019 coincidence spectroscopy of radicals produced in a flow tube: OH and OD, *J. Chem. Phys.*,
 1020 2015, **142**, 164201.
- 1021 66J. C. Poully, J. P. Schermann, N. Nieuwjaer, F. Lecomte, G. Grégoire, C. Desfrancois, G.
 1022 A. Garcia, L. Nahon, D. Nandi, L. Poisson and M. Hochlaf, Photoionization of 2-pyridone and
 1023 2-hydroxypyridine, *Physical Chemistry Chemical Physics*, 2010, **12**, 3566–3572.
- 1024 67M. Wartel, J.-F. Pauwels, P. Desgroux and X. Mercier, Quantitative measurement of
 1025 naphthalene in low-pressure flames by jet-cooled laser-induced fluorescence, *Applied Physics*
 1026 *B: Lasers and Optics*, 2010, **100**, 933–943.
- 1027 68T. S. Kasper, P. Oßwald, M. Kamphus and K. Kohse-Höinghaus, Ethanol flame structure
 1028 investigated by molecular beam mass spectrometry, *Combustion and Flame*, 2007, **150**, 220–
 1029 231.
- 1030 69N. Hansen, T. Kasper, S. J. Klippenstein, P. R. Westmoreland, M. E. Law, C. A. Taatjes, K.
 1031 Kohse-Höinghaus, J. Wang and T. A. Cool, Initial Steps of Aromatic Ring Formation in a
 1032 Laminar Premixed Fuel-Rich Cyclopentene Flame, *Journal of Physical Chemistry A*, 2007,
 1033 **111**, 4081–4092.

- 1034 70H.-S. Kim, D. R. Wagner and R. J. Saykally, Single Photon Infrared Emission Spectroscopy
1035 of the Gas Phase Pyrene Cation: Support for a Polycyclic Aromatic Hydrocarbon Origin of
1036 the Unidentified Infrared Emission Bands, *Phys. Rev. Lett.*, 2001, **86**, 5691–5694.
- 1037 71J. E. Elsila, N. P. de Leon and R. N. Zare, Factors Affecting Quantitative Analysis in Laser
1038 Desorption/Laser Ionization Mass Spectrometry, *Analytical Chemistry*, 2004, **76**, 2430–2437.
- 1039 72M. K. Spencer, M. R. Hammond and R. N. Zare, Laser mass spectrometric detection of
1040 extraterrestrial aromatic molecules: Mini-review and examination of pulsed heating effects,
1041 *PNAS*, 2008, **105**, 18096–18101.
- 1042 73P. M. Mayer, V. Blanchet and C. Joblin, Threshold photoelectron study of naphthalene,
1043 anthracene, pyrene, 1,2-dihydronaphthalene, and 9,10-dihydroanthracene, *J. Chem. Phys.*,
1044 2011, **134**, 244312.
- 1045 74G. Rouillé, S. Krasnokutski, D. Fulvio, C. Jäger, T. Henning, G. Garcia, X. Tang and L.
1046 Nahon, Dissociative photoionization of polycyclic aromatic hydrocarbon molecules carrying
1047 an ethynyl group, *The Astrophysical Journal*, , DOI:10.1088/0004-637X/810/2/114.
- 1048 75R. Boschi, E. Clar and W. Schmidt, Photoelectron spectra of polynuclear aromatics. III. The
1049 effect of nonplanarity in sterically overcrowded aromatic hydrocarbons, *J. Chem. Phys.*, 1974,
1050 **60**, 4406–4418.
- 1051 76M. J. S. Dewar, E. Haselbach and S. D. Worley, Calculated and observed ionization potentials
1052 of unsaturated polycyclic hydrocarbons; calculated heats of formation by several
1053 semiempirical s. c. f. m.o. methods, *Proceedings of the Royal Society of London. A.*
1054 *Mathematical and Physical Sciences*, 1970, **315**, 431–442.
- 1055 77M. Meot-Ner, Ion thermochemistry of low-volatility compounds in the gas phase. 3.
1056 Polycyclic aromatics: ionization energies, proton and hydrogen affinities. Extrapolations to
1057 graphite, *J. Phys. Chem.*, 1980, **84**, 2716–2723.
- 1058 78M. Kinoshita, The Absorption Spectra of the Molecular Complexes of Aromatic Compounds
1059 with p-Bromanil, *BCSJ*, 1962, **35**, 1609–1611.
- 1060 79E. Heilbronner, T. Hoshi, J. L. von Rosenberg and K. Hafner, Alkyl-induced, natural
1061 hypsochromic shifts of the 2A←2X and 2B←2X transitions of azulene and naphthalene
1062 radical cations, *Nouv. J. Chim.*, 1976, **1**, 105.
- 1063 80Y. Ling and C. Lifshitz, Time-Dependent Mass Spectra and Breakdown Graphs. 19.
1064 Fluoranthene, *J. Phys. Chem.*, 1995, **99**, 11074–11080.
- 1065 81M. A. Slifkin and A. C. Allison, Measurement of Ionization Potentials from Contact Charge
1066 Transfer Spectra, *Nature*, 1967, **215**, 949–950.
- 1067 82Y. Li, L. Zhang, T. Yuan, K. Zhang, J. Yang, B. Yang, F. Qi and C. K. Law, Investigation on
1068 fuel-rich premixed flames of monocyclic aromatic hydrocarbons: Part I. Intermediate
1069 identification and mass spectrometric analysis, *Combustion and Flame*, 2010, **157**, 143–154.
- 1070 83L. Klasinc, B. Kovac and H. Gusten, Photoelectron spectra of acenes. Electronic structure and
1071 substituent effects, *Pure and Applied Chemistry*, 1983, **55**, 289–298.
- 1072 84E. Heilbronner, R. Gleiter, H. Hopf, V. Hornung and A. De Meijere, Photoelectron-
1073 Spectroscopic Evidence for the Orbital Sequence in Fulvene and 3, 4-Dimethylene-
1074 cyclobutene, *Helvetica Chimica Acta*, 1971, **54**, 783–794.
- 1075 85P. A. Clark, F. Brogli and E. Heilbronner, The π -Orbital Energies of the Acenes, *Helvetica*
1076 *Chimica Acta*, 1972, **55**, 1415–1428.
- 1077 86T. A. Cool, J. Wang, K. Nakajima, C. A. Taatjes and A. McIlroy, Photoionization cross
1078 sections for reaction intermediates in hydrocarbon combustion, *International Journal of Mass*
1079 *Spectrometry*, 2005, **247**, 18–27.
- 1080 87E. E. Rennie, C. a. F. Johnson, J. E. Parker, D. M. P. Holland, D. A. Shaw and M. A. Hayes,
1081 A photoabsorption, photodissociation and photoelectron spectroscopy study of C₆H₆ and
1082 C₆D₆, *Chemical Physics*, 1998, **229**, 107–123.

- 1083 88S. Soorkia, A. J. Trevitt, T. M. Selby, D. L. Osborn, C. A. Taatjes, K. R. Wilson and S. R.
1084 Leone, Reaction of the C₂H Radical with 1-Butyne (C₄H₆): Low-Temperature Kinetics and
1085 Isomer-Specific Product Detection, *J. Phys. Chem. A*, 2010, **114**, 3340–3354.
- 1086 89P. Carlier and G. Mouvier, Etude par spectrometrie de photoelectrons de la structure
1087 electronique des phenyl-alcynes conjugués, *Journal of Electron Spectroscopy and Related*
1088 *Phenomena*, 1979, **16**, 169–181.
- 1089 90B. West, A. Sit, A. Bodi, P. Hemberger and P. M. Mayer, Dissociative Photoionization and
1090 Threshold Photoelectron Spectra of Polycyclic Aromatic Hydrocarbon Fragments: An
1091 Imaging Photoelectron Photoion Coincidence (iPEPICO) Study of Four Substituted Benzene
1092 Radical Cations, *The Journal of Physical Chemistry A*, 2014, **118**, 11226–11234.
- 1093 91F. Zhang, R. I. Kaiser, V. V. Kislov, A. M. Mebel, A. Golan and M. Ahmed, A VUV
1094 Photoionization Study of the Formation of the Indene Molecule and Its Isomers, *J. Phys.*
1095 *Chem. Lett.*, 2011, **2**, 1731–1735.
- 1096 92C. R. Brundle, M. B. Robin and N. A. Kuebler, Perfluoro effect in photoelectron
1097 spectroscopy. II. Aromatic molecules, *J. Am. Chem. Soc.*, 1972, **94**, 1466–1475.
- 1098 93D. Dougherty, J. Lewis, R. V. Nauman and S. P. McGlynn, Photoelectron spectroscopy of
1099 azulenes, *Journal of Electron Spectroscopy and Related Phenomena*, 1980, **19**, 21–33.
- 1100 94C.-H. Chin, T. Zhu and J. Z. Zhang, Theoretical Investigations of Photoionization Efficiency
1101 of Naphthalene, , DOI:10.26434/chemrxiv.7665620.v1.
- 1102 95R. Gleiter, W. Schäfer and M. Eckert-Maksić, Transannulare Wechselwirkungen zwischen
1103 Acetylenen – Photoelektronenspektroskopische Untersuchungen an 1,8-Diethylnaphthalin
1104 und cyclischen Derivaten von 2,2'-Diethylnylbiphenyl, *Chemische Berichte*, 1981, **114**, 2309–
1105 2321.
- 1106 96Y. Y. Li, Y. JiuZhong and C. ZhanJun, Photonionization Cross Section Database (Version
1107 2.0)., <http://flame.nslr.ustc.edu.cn/database/>.
- 1108 97J. Appel, H. Bockhorn and M. Wulkow, A detailed numerical study of the evolution of soot
1109 particle size distributions in laminar premixed flames, *Chemosphere*, 2001, **42**, 635–645.
- 1110 98N. A. Eaves, S. B. Dworkin and M. J. Thomson, Assessing relative contributions of PAHs to
1111 soot mass by reversible heterogeneous nucleation and condensation, *Proceedings of the*
1112 *Combustion Institute*, 2017, **36**, 935–945.
- 1113 99C. A. Schuetz and M. Frenklach, Nucleation of soot: Molecular dynamics simulations of
1114 pyrene dimerization, *Proceedings of the Combustion Institute*, 2002, **29**, 2307–2314.
- 1115 100 R. Boschi and W. Schmidt, Photoelectron spectra of polycyclic aromatic hydrocarbons.
1116 Pyrene and coronene, *Tetrahedron Letters*, 1972, **13**, 2577–2580.
- 1117 101 K. O. Johansson, T. Dillstrom, P. Elvati, M. F. Campbell, P. E. Schrader, D. M. Popolan-
1118 Vaida, N. K. Richards-Henderson, K. R. Wilson, A. Violi and H. A. Michelsen, Radical–
1119 radical reactions, pyrene nucleation, and incipient soot formation in combustion, *Proceedings*
1120 *of the Combustion Institute*, 2017, **36**, 799–806.
- 1121 102 B. D. Adamson, S. A. Skeen, M. Ahmed and N. Hansen, Detection of Aliphatically
1122 Bridged Multi-Core Polycyclic Aromatic Hydrocarbons in Sooting Flames with Atmospheric-
1123 Sampling High-Resolution Tandem Mass Spectrometry, *J. Phys. Chem. A*, 2018, **122**, 9338–
1124 9349.
- 1125 103 J. W. Martin, D. Hou, A. Menon, L. Pascazio, J. Akroyd, X. You and M. Kraft,
1126 Reactivity of Polycyclic Aromatic Hydrocarbon Soot Precursors: Implications of Localized π -
1127 Radicals on Rim-Based Pentagonal Rings, *J. Phys. Chem. C*, 2019, **123**, 26673–26682.
- 1128 104 R. A. Krueger and G. Blanquart, Predicting aromatic exciplex fluorescence emission
1129 energies, *Phys. Chem. Chem. Phys.*, 2019, **21**, 10325–10335.

1131